~~Event-based analysis of extreme precipitation trends in~~ Hourly Precipitation Patterns and Extremization over Italy using ~~hourly~~ convection-permitting ~~reanalyses~~reanalysis data

Francesco Cavalleri[1,2], Cristian Lussana[3], Francesca Viterbo[2], Michele Brunetti[4], Riccardo Bonanno[2], Veronica Manara[1], Matteo Lacavalla[2], and Maurizio Maugeri[1]

[1]Environmental Science and Policy Department (ESP), University of Milan, Milan, 20133, Italy
[2]Sustainable Development and Energy Resources Department, Research on Electric Systems (RSE), Milan, 20134, Italy
[3]Division for Climate Services, the Norwegian Meteorological Institute, Oslo, 0313, Norway
[4]Institute of Atmospheric Sciences and Climate, National Research Council (CNR-ISAC), Bologna, 40129, Italy

Correspondence: Francesco Cavalleri (francesco.cavalleri@unimi.it)

Abstract. The latest generation of ~~high-resolution and~~ convection-permitting reanalyses, capable of representing atmospheric processes at small spatial scales (≤4 km), is crucial for studying the temporal and spatial evolution of phenomena such as convective storms and orographic precipitation. Given the ~~availability of long (>35~~ long (37 years) and continuous availability of the MERIDA HRES convection-permitting reanalysis datasets over Italy, this study ~~investigates the occurrence and characteristics of hourly extreme precipitation events (EPEs) and quantifies their potential~~ employs its precipitation fields to investigate hourly precipitation patterns, extremes, and quantify their increase over time in this region. ~~Using the MERIDA HRES reanalysis (1986–2022), precipitation events~~ Precipitation clusters are extracted from hourly reanalysis fields as spatially coherent structures, yielding approximately 160,000 ~~events per year. Each event is~~ of them per year, each one characterized by intensity and shape indicators. The resulting ~~HOPE-X~~ HOPSS-X (HOurly Precipitation ~~Events and Xtremes~~Spatial Structures and eXtremes) dataset enables a detailed climatological analysis of ~~event~~ hourly precipitation frequency, intensity, and spatial ~~scale across seasons. The most extreme component of those events (EPEs) , defined based~~ extent across different seasons and regions. The Hourly Precipitation Extremes (HPEs) are selected from this dataset basing on the mean of local annual maxima in hourly precipitation (RX1hour)~~, show a pronounced increase in occurrence. Specifically, significant upward trends~~ . Significant upward trends in HPEs occurrences (+20% / +30%) are present during summer in several Alpine and Prealpine regions, as well as in parts of Calabria. In autumn, ~~significant signals~~ similar signals (+30% / +40%) emerge in the southern Apennines and in coastal and maritime areas, including the eastern Ligurian coast, eastern Sardinia, the southern Adriatic Sea, and the Ionian Sea. These spatial and seasonal patterns align with regions where convective processes predominantly drive intense, localised precipitation, potentially amplified by climate change. While these findings should be considered in light of known limitations of reanalysis products, such as spatial mismatches with observations and temporal inhomogeneities, multiple independent observational studies support the increase in ~~EPEs~~ HPEs during summer and autumn in specific areas. Moreover, the methodology presented here is broadly applicable in any region with access to long-term convection-permitting reanalysis data. In summary, ~~this study offers~~ the purpose of this study is to offer a contribution to the ongoing discussion on precipitation extremes and

trends in Italy and ~~provides~~ provide guidance for leveraging reanalysis data to enhance infrastructure resilience to short-lived, intense precipitation events.

1 Introduction

As global temperatures continue to rise due to climate change (IPCC, 2023), significant alterations in large-scale precipitation patterns are being observed across the globe (Allan et al., 2020). These shifts can trigger even more pronounced changes at the local level (Fowler et al., 2021), particularly in the frequency, intensity, and timing of ~~Extreme Precipitation Events (EPEs)~~extreme precipitation. The physical reason for these changes lies in the Clausius-Clapeyron thermodynamic relationship (Hardwick Jones et al., 2010), which describes how a warmer atmosphere can hold more water vapour. Moreover, the rising ocean temperature observed in recent decades (Garcia-Soto et al., 2021) provides more moisture to fill the atmospheric column. ~~The increase in moisture availability produces contrasting effects (Zaitchik et al., 2023)~~Climate change produces however contrasting effects: some regions may experience drier conditions, while others may see more intense and frequent rainfall ~~, including extreme precipitation events (EPEs) . This effect is~~ (Zaitchik et al., 2023). Both drying and wetting regions may experience changes in extreme precipitation (Donat et al., 2017). The thermodynamic effects tend to produce a relatively uniform increase in precipitation extremes, but dynamic contributions (such as orography, coastal interaction, and changes in weather regimes) can modulate these changes regionally, leading to local variations in the intensity and frequency of extremes (Pfahl et al., 2017). Moreover, such extremes are generally more pronounced at shorter timescales, such as hourly, than at longer durations (Lenderink et al., 2017).

The Mediterranean region, in particular, is recognised as a climate change hotspot, undergoing warming at a faster rate than many other parts of the world (Lionello and Scarascia, 2018). The increasing sea surface temperatures in the Mediterranean contribute to more frequent heavy precipitation events (Senatore et al., 2025), in particular ~~over the Alps and for hourly timescales~~ at the hourly timescale (Peleg et al., 2025). Within this region, Italy is especially vulnerable to ~~EPEs~~ short-lived extreme precipitation. (Giovannini et al., 2021; Donnini et al., 2023; Padulano et al., 2019), largely due to its complex orography and the dynamical interaction between moist air masses, mountain chains, and coastal ~~dynamics~~ interface (Stocchi and Davolio, 2017; Mazzoglio et al., 2022). All these aspects highlight the need to investigate whether and to what extent climate change is impacting the distribution of hourly precipitation extremes over Italy.

Research on precipitation trends in Italy has been extensive over the past decades, revealing a complex spatial and temporal variability shaped by regional climatic dynamics, topography, and large-scale atmospheric patterns. Several regional investigations based on observational datasets contributed to this discussion, emphasising pronounced local differences. Caloiero et al. (2018, 2021) reported significant negative trends for the period 1951–2016 in both seasonal and annual total rainfall in Southern Italy and inland central regions, especially in winter and autumn. Similarly, in Trentino-Alto Adige (north-eastern Italy), Brugnara et al. (2012) observed a decrease in annual precipitation on the order of 1.0–1.5% per decade in the period

1922-2009, with spring and winter contributing most to the decline. In the same study, the number of wet days significantly decreased east of the Adige Valley (north-western Italy), while trends in extremes (90th, 95th, 99th percentiles) were weak and mostly non-significant. In Tuscany (west-central Italy), Bartolini et al. (2014) found a declining trend in annual rainfall and wet days for the period 1955-2007, largely due to winter and spring decreases. In Calabria (southern Italy), Brunetti et al. (2012), using a high-resolution daily dataset for the period 1923–2006, detected negative trends in mean precipitation intensity (total precipitation per wet day), a reduction in daily precipitation amounts, and a decreased frequency of high-intensity daily events (95th and 99th percentiles). Similarly, Pavan et al. (2019), analysing the ~~ARCIS gridded observational dataset for northern Italy~~*Archivio Climatologico per l'Italia Centro Settentrionale* (ARCIS), a high-resolution gridded precipitation dataset for north-central Italy, for the period ~~1961-2015, found~~ 1961–2015, found widespread summer declines in most regions—driven by fewer rainy days, longer dry spells, and reduced daily intensity—except ~~for~~ in the northern Alpine area, ~~which showed increases in~~ where both total and intense precipitation increased. Finally, Capozzi et al. (2023) analysed multiple stations across Campania (south-western Italy) for the period 2002–2021 and found an increasing trend in both precipitation intensity and the frequency of heavy rainfall events during autumn, particularly in the northern part of the region and in mountainous areas.

Collectively, these studies ~~depict a complex~~ show a complex and heterogeneous evolution of precipitation regimes in Italy~~, marked by substantial heterogeneity~~. However, ~~it is important to note that these studies rely on observational datasets with daily resolution, while the primary effects of climate change~~ they are based on daily datasets, whereas climate change impacts on precipitation are most evident at sub-daily timescales (Lenderink et al., 2017). ~~Indeed, sub-daily observational datasets typically~~ Sub-daily observational datasets usually cover limited regions and ~~relatively short periods, and are generally unavailable for longer durations while also providing full national~~ rarely provide long-term, nationwide coverage (Blenkinsop et al., 2018; Morbidelli et al., 2025). In Italy, the observational network is extensive and of high quality, but since the 1990s it has been managed at the regional level, resulting in some heterogeneity among measurement networks. ~~An attempt to homogenize sub-daily observations was made through the development of the GRIPHOdataset (Fantini, 2019); however,~~ The GRidded Italian Precipitation Hourly Observations (GRIPHO) dataset (Fantini, 2019) was developed to homogenize hourly observations, but its limited temporal coverage (2001–2016) ~~makes it unsuitable~~ restricts its usefulness for long-term trend ~~analysis~~analyses. Consequently, sub-daily precipitation trends can be investigated using observations available for specific regions ~~. For example, a delay in the timing~~ only. Regional analyses show a delay of sub-daily rainfall extremes toward autumn ~~was observed in Emilia-Romagna, along with an overall increase in event magnitude , particularly in the Apennine region (Persiano et al., 2020). In southern Italy , a growing tendency in hourly extreme rainfall events was observed at several locations, and these trends generally loose significance over~~ and increasing event magnitude in Emilia-Romagna (Persiano et al., 2020), while southern Italy exhibits rising hourly extremes whose significance decreases at longer durations (Avino et al., 2024). ~~Notably, Mazzoglio et al. (2020) developed a national dataset of annual daily and sub-daily precipitation maxima for the period~~ Mazzoglio et al. (2020) developed the I2-RED dataset (1916~~to~~ –2022~~(I2-RED), finding that~~), showing

nationwide increases in annual maxima for short durations (particularly 1-hour)have increased nationwideespecially 1 h). In contrast, longer durations, such as 24-hour aggregations, exhibit more spatially variable trends, including some negative tendencies (Mazzoglio et al., 2025). Furthermore, the authors highlight that the highest quantiles (0.95–0.99) display larger changes than median values. These findings underscore the need for innovative methodologies to effectively capture and interpret evolving patterns in hourly extreme precipitation across Italy, beyond observations alone. In fact, This is also because rain gauge networks often lack the spatial density required to detect needed to capture highly localised events, such as convective storms, unless they occur directly over a station, and consequently they tend to underestimate extremes by about 20% (Schroeer et al., 2018). Conversely, radar and satellite-based measurementsprecipitation estimates, while offering broader spatial coverage, may suffer from biasescan exhibit substantial positive or negative biases, particularly during high-intensity events or be in areas affected by terrain-induced signal blocking (Wang et al., 2021). For this reason, convection-permitting reanalyses, blending model outputs with observational data, have proven to be valuable tools for investigating EPEs precipitation extremes and assessing their potential trends over time (Dallan et al., 2024; Poschlod et al., 2021).

In this context, this study aims to investigate the spatial and seasonal characteristics of hourly precipitation events over Italy and to assess potential changes over timein its most extreme componentcontribute to the ongoing scientific discussion on precipitation trends and extremes by proposing a methodological framework for an informed use of convection-permitting reanalysis data to characterise hourly precipitation structures across space and seasons, and to investigate the potential precipitation extremization over time. To this end, the hourly precipitation fields from the convection-permitting MEteorological Reanalysis Italian DAtaset – High RESolution, MERIDA HRES (Viterbo et al., 2024) are employed. This product covers , covering the 37-year period from 1986 to 2022 at about a 4 km resolution. The choice of MERIDA HRES is supported by previous validation studies that have demonstrated the product's reliability. Its precipitation fields have been assessed from climatological to daily (Cavalleri et al., 2024a; Viterbo et al., 2024) and hourly (Giordani et al., 2025) timescales. Other studies have inter-compared the performance of many reanalyses over Italy, including MERIDA HRES, highlighting both their strengths and limitations in representing various meteorological variables (Bonanno et al., 2019; Raffa et al., 2021; Giordani et al., 2023; Cavalleri et al., 2024b) . MERIDA HRES has been proven capable of representing convective features of precipitation at fine spatial scales, showing good agreement with both gridded and station-based observations, and demonstrating overall temporal stability when compared with homogenised observational datasets (Cavalleri et al., 2024a). These qualities make it the most appropriate product for hourly precipitation trend analyses. Other convection-permitting models available for Italy, such as MOLOCH (Capecchi et al., 2023) and SPHERA (Cerenzia et al., 2022; Giordani et al., 2023), have been found to generally produce larger deviations from observed precipitation trends than MERIDA HRES (Cavalleri et al., 2024a), while results from VHR-REA_IT (Raffa et al., 2021) indicate a slightly weaker agreement with daily-scale observations (Cavalleri et al., 2024a). These aspects may limit their applicability for the event-based analysis presented in this study.

Even if convection-permitting reanalyses represent a state-of-the-art, precipitation remains one of the most challenging variables to simulate, and it is not directly assimilated by the reanalyses, but instead derived from assimilated variables such as temperature, pressure, and humidity. These limitations ~~, together with the inherently chaotic nature of the atmosphere, especially at small scales (Hohenegger and Schär, 2007),~~ often lead to some discrepancies between simulated and observed precipitation fields at the smaller scales, especially during summer, mainly due to precipitation positioning uncertainties (Cavalleri et al., 2024a). This issue also arises from the inherently chaotic nature of the atmosphere (Hohenegger and Schär, 2007) together with limitations in the data assimilation frequency ~~(Kalnay et al., 2024)~~ of the driving global reanalyses (Kalnay et al., 2024) (e.g., ERA5 assimilates data every 12 hours, much less than typical timescales of convection). ~~While the assimilated~~ Assimilated observations remain the same regardless of the ~~temporal scale, the sub-daily precipitation fields no longer benefit from the temporal aggregation , which~~ investigated temporal scale. Temporal aggregation (e.g. daily) can sometimes hide deficiencies at a smaller scale. At the sub-daily scale (e.g. hourly) precipitation fields no longer benefit from this effect, making deviations from observations more noticeable. Another relevant aspect is the potential divergence in precipitation trends between observations and reanalyses. Discrepancies in ~~the decadal trend~~ trends of annual precipitation totals were highlighted in global reanalyses (Lussana et al., 2024) and Italian regional ones (Cavalleri et al., 2024a).

In light of these limitations, an ~~event-based approach~~ approach based on precipitation structures has been adopted to mitigate positioning uncertainties issues. In particular, in this work spatially continuous hourly precipitation structures and associated extremes are identified through the use of a clustering technique. Clustering methods are commonly employed to identify individual precipitation ~~events~~ structures from gridded datasets, particularly in the context of radar-based observations and operational verification. These techniques typically rely on threshold-based object identification combined with clustering algorithms to isolate spatially coherent precipitation structures. For example, Wernli et al. (2008) describe an object-based verification method (SAL) that requires the identification of distinct precipitation objects using a threshold proportional to the domain's maximum precipitation value, a strategy also discussed by Davis et al. (2006). Marzban and Sandgathe (2006) provide a broader review of clustering approaches applied to precipitation fields, showing how cluster analysis can be used to define features or objects in both forecast and observation fields, enabling ~~event-based verification. Beyond verification~~verification. Moreover, clustering methods have also been applied to classify sub-daily rainfall ~~events~~ episodes according to their internal structure (Sottile et al., 2022). Several methods have also been developed to track precipitation events over time (Chang et al., 2016; White et al., 2017; Li et al., 2020). In this study, however, a straightforward approach to identify precipitation ~~clusters~~ structures is proposed, ~~based on percentile thresholds that adapt to seasonal variability and the differing precipitation regimes across regions. This methodology does not account~~ not accounting for the temporal evolution of the ~~events identified within each cluster but rather focuses~~ precipitation events, focusing on each hourly time step independently~~, being fully aware of the limitations of this approach, as discussed and acknowledged in the following~~.

~~The paper presents in Section 2 the reanalysis dataset used in this study (MERIDA HRES) and~~ The paper is organized as follows. Section 2 introduces the MERIDA HRES reanalysis, detailing the reasons for its selection along with its inherent strengths and limitations, and describes the methodology adopted to construct the HOurly Precipitation ~~Events~~ Spatial Structures and Xtremes (~~HOPE-X~~HOPSS-X) dataset, publicly available on Zenodo at https://bit.ly/HOPSS-X. Section 3 outlines the main results, focusing on the spatial distribution and seasonal patterns of hourly precipitation ~~events~~structures, with particular emphasis on the ~~EPEs~~ extremes subset and related trends. Section 4 discusses these findings in the context of previous studies on precipitation trends and known limitations of reanalysis data. Finally, Section 5 summarises the key conclusions and outlines potential directions for future research.

2 Data and Methods

2.1 MERIDA HRES, a convection-permitting reanalysis

This study employs the hourly precipitation fields from MERIDA HRES (Viterbo et al., 2024), a reanalysis developed for the Italian domain, resolving explicit convection to better represent localised and intense precipitation events. MERIDA HRES, developed by ~~Ricerca sul Sistema Energetico~~ *Ricerca sul Sistema Energetico* (RSE), employs the Weather Research and Forecasting (WRF) model to dynamically downscale over Italy the global ERA5 reanalysis (Hersbach et al., 2020) to a ~~high-resolution~~ higher-resolution horizontal grid of approximately 4 km ~~over Italy~~and 56 vertical levels, with increased vertical resolution in the lower atmosphere (levels located at 10, 35, 70, 100, 130, 180, 250, 325, 415, and 500 m). It is driven by large-scale initial and boundary conditions from ERA5 and applies a spectral nudging technique (von Storch et al., 2000) to constrain synoptic-scale features while filtering out smaller-scale perturbations that could introduce spurious signals. Additionally, SYNOP surface air temperature observations are assimilated through an observational nudging technique (Liu et al., 2012; Bonanno et al., 2019; Viterbo et al., 2024), further enhancing the representation of regional atmospheric characteristics. The dataset spans the period from 1986 to 2022, but is constantly updated with about a ~~2-year~~ two-year lag. The analyses for this work are calculated over the domain 5.84°E to 18.96°E ~~in longitude~~ and 35.37°N to 48.25°N, centred on the Italian peninsula, for the period 1986-2022, enclosing the full period of availability for MERIDA HRES at the time of writing.

2.2 ~~Event detection and characterization~~

The specific choice of MERIDA HRES reanalysis is supported by previous validation studies. In particular, its precipitation fields have been assessed from climatological to daily (Cavalleri et al., 2024a; Viterbo et al., 2024) and hourly (Giordani et al., 2025) timescales, also comparing with other convection-permitting reanalyses for the same area, highlighting both its strengths and limitations. The effective horizontal spatial resolution of MERIDA HRES has been evaluated in previous works using a wavelet spectral decomposition approach (see Cavalleri et al. (2024a), Fig. 2), which demonstrated its ability to represent convective precipitation, although it may not fully resolve the smallest structures. Moreover, MERIDA HRES shows good agreement with both gridded and station-based observations, and demonstrates overall temporal stability when compared with homogenised

observational datasets (Cavalleri et al., 2024a). These qualities make it an appropriate product for hourly precipitation trend analyses. Other convection-permitting models available for Italy, such as MOLOCH (Capecchi et al., 2023) and SPHERA (Cerenzia et al., 2022; Giordani et al., 2023), have been found to generally produce larger deviations from observed precipitation trends than MERIDA HRES (Cavalleri et al., 2024a), while results from VHR-REA_IT (Raffa et al., 2021) indicate a slightly weaker agreement with daily-scale observations (Cavalleri et al., 2024a). These aspects may limit the applicability of other products in this study.

Nevertheless, these studies also indicate that MERIDA HRES occasionally overestimates rainfall amounts during summer in specific regions, including the Po Valley–Adriatic interface, parts of the Calabrian mountains, southern Apulia, and the southern portions of the main islands, with local deviations from observations reaching 10–30 mm. However, since these regions are generally dry during summer, the relative error can be substantial, up to locally doubling the observed rainfall amounts in July and August (Cavalleri et al., 2024a). Moreover, the trend in the annual differences between MERIDA HRES and homogenised observations precipitation totals is on average 4% per decade, meaning that this fraction of annual precipitation increase might be attributable to a deviation from observations rather than a true climate signal (Cavalleri et al., 2024a). This mismatch is not uniform across the territory (see the supplementary material of Cavalleri et al. (2024a)). The knowledge of these specific inhomogeneities of MERIDA HRES will be taken into account when discussing the results of this work (Section 4).

2.2 Precipitation structures detection and characterization

~~The event-detection method used in this study aims to identify spatially coherent precipitation events from each~~

The first step involves identifying coherent Hourly Precipitation Spatial Structure (HPSSs) in each MERIDA HRES hourly field. ~~It applies the 50th percentile of precipitation values exceeding 1 mm as a threshold, computed~~ To account for seasonal and regional differences, thresholds are calculated for each grid point of the ~~MERIDA HRES reanalysis . Thresholds are calculated~~ reanalysis and separately for each season ~~. Finally~~by taking the median (i.e., 50th percentile) of precipitation values exceeding 1 mm. After that, a spatial smoothing filter with a 20 km radius is applied to reduce noise and improve spatial consistency across neighbouring grid cells (Figure 1).

Precipitation values below 1 mm/h are excluded to distinguish meaningful precipitation from background noise. ~~Below this value,~~ Indeed, below 1 mm/h the spatial variability is very high, whereas it significantly decreases above it, indicating that precipitation becomes more spatially coherent and representative of broader areas (Lussana et al., 2023). ~~At the beginning~~During the first stages of this work, a fixed 1 mm threshold was applied to detect ~~hourly precipitation events~~HPSS. Nevertheless, the choice of a uniform threshold across the entire domain and for all seasons did not adequately account for the spatial and seasonal variability of precipitation regimes, leading to the merging of multiple distinct convective cells into a single, large cluster that did not reflect the localised nature of ~~these events~~HPSSs. This mismatch between the actual physical scale of convective systems and the scale of the detected clusters motivated the choice of a percentile-based threshold~~, computed using all hourly precipitation values greater than 1 mm, separately for each season. The thresholds, defined as the 50th percentile of precipitation above 1 mm (Figure 1), are applied to all hourly precipitation fields from 1986 to 2022.~~ . In determining the most suitable smoothing radius, several values were tested. Radii larger than 20 km excessively smoothed areas with

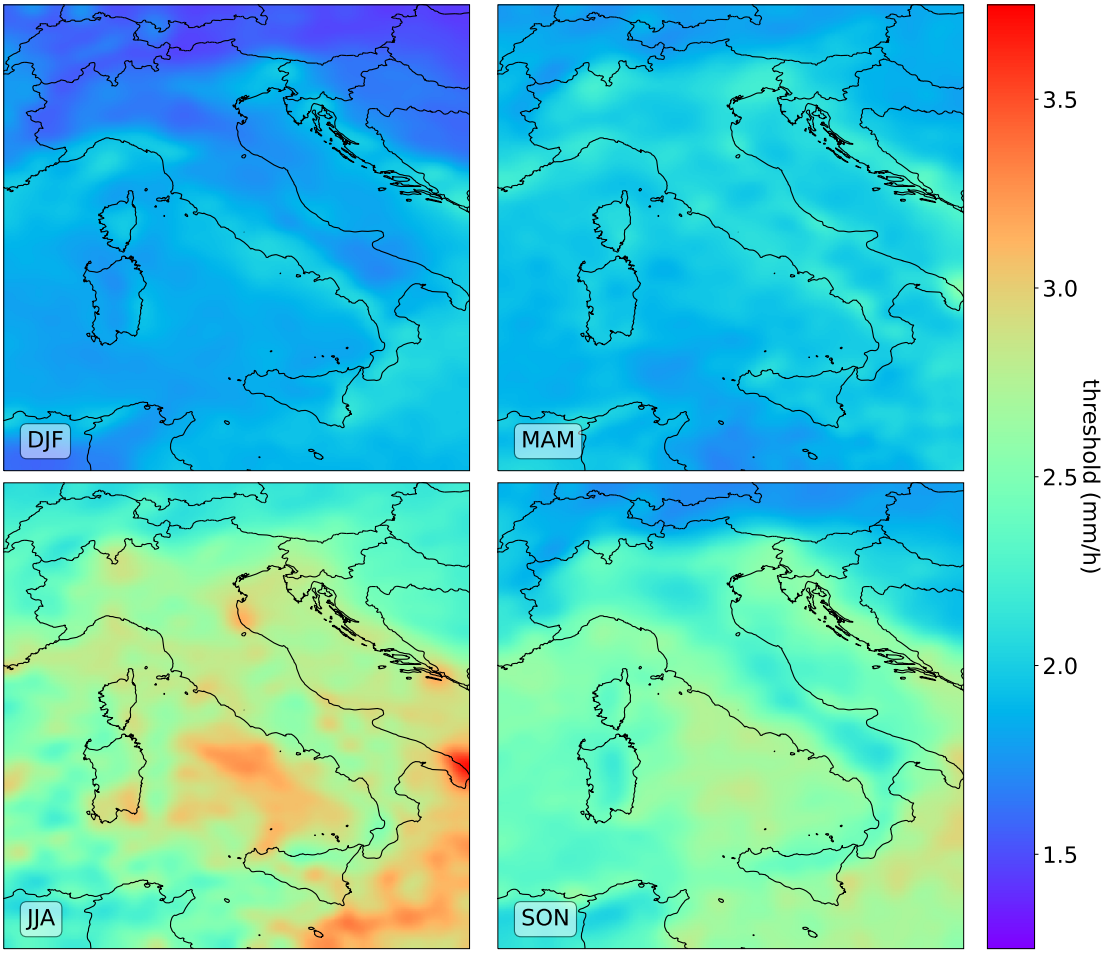

Figure 1. Seasonal maps of the ~~50th percentile~~ median of hourly precipitation values above 1 mm, used as ~~clustering~~ thresholds.

higher thresholds, reducing the ability to resolve regions of intense precipitation. Conversely, smaller radii retained too much noise, limiting the effectiveness of the thresholds in isolating coherent precipitation structures. Moreover, 20 km approximately corresponds to the boundary between the meso-β and meso-γ atmospheric scales (Thunis and Bornstein, 1996), below which convective phenomena typically occur.

Contiguous grid points exceeding ~~these thresholds are identified~~ the thresholds (Figure 1) are treated as an individual ~~event~~cluster. To reduce noise, clusters composed of fewer than five grid points are excluded: approximately 95% of them exhibit intensities below 10 mm/h, and therefore have a negligible impact on the focus of this study on extreme precipitation. ~~Retained clusters are identified as individual relevant precipitation events~~Each retained cluster is identified as an HPSS. More specifically, ~~'relevant' refers to spatially continuous precipitation structures that occur in more than half of the instances within~~ in this work HPSSs are spatially continuous hourly precipitation structures, identifying detectable and relevant precipitation

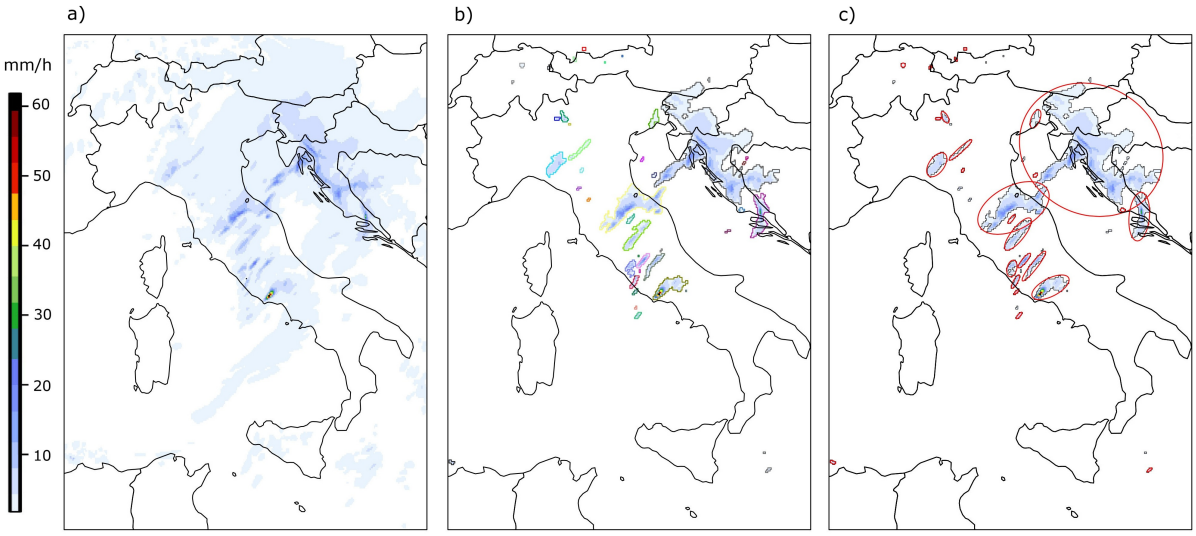

Figure 2. Example of HPSS detection process for the day 20th October 2011, 13:00:00 UTC. a) raw precipitation field, b) after applying the threshold and the clustering (each border colour represents a different cluster), c) minimum enclosing ellipses (in red) identify retained structures.

with reference to a given area and season~~, and are therefore considered sufficient to identify detectable, and at times significant, events. Hereafter, the term 'event' denotes the precipitation structures identified using this method.~~ . Figure 2 shows an example of the ~~event-detection procedure~~ procedure used to identify HPSSs, applied to the hourly precipitation field of 20 October 2011 at 13:00:00 UTC. On that day, intense precipitation affected Rome and the surrounding areas, causing several floods throughout the city and widespread power outages (Bonanno et al., 2019).

~~Example of event selection process for the day 20th October 2011, 13:00:00 UTC. a) raw precipitation field, b) after applying the threshold and the clustering (each border colour represents a different cluster), c) minimum enclosing ellipses (in red) identify retained events.~~

~~For each identified event, an enclosing ellipse is calculated following the methodology of Wernli et al. (2008), and key properties are extracted. The characteristics and methods used for their calculation are summarised and explained in Table~~Each identified HPSS is characterized by a set of features describing its date and time of occurrence, position, and total and maximum precipitation intensity, as summarized in Table 1. The ~~table presents only the characteristics directly used in this study; however, many additional variables~~ maximum linear spatial extent of a HPSS is defined as the major axis of its minimum enclosing ellipse — i.e., the smallest ellipse that fully contains all grid points belonging to the structure (Wernli et al., 2008). The choice of characterizing the shape of an HPSS by its maximum linear extent is motivated by the fact that atmospheric spatial scales are generally defined in linear terms (Thunis and Bornstein, 1996). Moreover, deriving this feature from the minimum enclosing

ellipse allows for a consistent characterization of precipitation structure having very different shapes. Additional features are included in the complete database available only, while only features used in this study are reported here.

Table 1. The ~~characteristics~~ set of feature recorded for each ~~event~~ HPSS which are relevant for this study.

~~Variable Name~~Feature name in the database	Description and/or definition	Un
time	Date and hour of the field where the ~~object is detected .~~ HPSS is detected	-
tp_max	Maximum ~~total~~ hourly precipitation value within the ~~object.~~ HPSS	mm
lon_max	Longitude where ~~maximum precipitation (~~tp_max ~~) occurs .~~ occurs	deg
lat_max	Latitude where ~~maximum precipitation (~~tp_max ~~) occurs .~~ occurs	deg
~~lon~~cdm_~~wavg~~lon	Intensity-weighted average longitude of the ~~object.~~ HPSS	deg
~~lat~~cdm_~~wavg~~lat	Intensity-weighted average latitude of the ~~object. area~~ HPSS	~~Ar~~
tot_tp	~~Total~~ Hourly precipitation summed over ~~the entire object area.~~ all points composing the HPSS	mm
~~axis_maj~~area	Number of pixels composing the HPSS	-
max_extent	Length of the major axis of the ~~object (in degrees).~~ HPSS minimum enclosing ellipse	deg

2.3 ~~Event-based~~ Structure-based statistics

The ~~event detection methodology explained above resulted in the HOPE-X dataset. Several indicators are computed from this dataset. First,~~ HPSS detection methodology described above produced the HOPSS-X dataset, which can be analysed through the set of features associated with each HPSS. First, the seasonal distributions of ~~selected characteristics listed in Table 1 are obtained to provide an overview of their values. In particular, the average intensity (~~tot_tp/area~~~~mean precipitation intensity (tot_tp / area), peak ~~intensity (~~tp_max~~~~precipitation intensity (tp_max), and ~~spatial scale (~~axis_maj~~) of individual events~~ maximum linear spatial extent (max_extent) of all HPPS are examined. Then, spatial patterns of hourly precipitation are investigated~~, accounting~~ . To account for location uncertainty inherent in reanalysis data ~~. To this end, a spatial aggregation is applied using a moving window of~~ and avoid misleading point-scale analyses, statistics are not evaluated at individual grid points but within a 0.5° moving window (≈156 grid points) with 0.1° increments in both latitude and longitude. In each of these windows, the ~~number of events~~ Number of occurrences (N) of HPSSs whose centre of mass (~~lat_wavg,lon_wavg~~cdm_lat,cdm_lon) fell inside the window is counted. Because the sliding distance (0.1°) is smaller than the window size (0.5°), a single ~~event~~ HPSS is counted in multiple adjacent windows, ensuring smooth spatial transitions. ~~The Average Intensity (AvIn), the~~ Then, some features are averaged among all the HPSSs falling in a window. Specifically, the Average Mean Intensity (MeanInt), Average Peak Intensity (~~PkIn~~PeakInt), and ~~Spatial Scale (SpS~~Average Maximum Linear Spatial Extent (SpatExtent) are obtained by averaging ~~over the events within each window~~ tot_tp/area, tp_max and ~~axis_maj~~ max_extent respectively, as detailed in Table 2.

Table 2. Description of indicators used for the analyses and their units of measure, where $t = 1, \ldots, T$ indicates the different hours within the period over which the indicator is computed (typically a season), and $m = 1, \ldots, M$ denotes the different ~~events~~ HPSSs occurring at a timestep within a given spatial window.

Short Name	Indicator Full Name	Mathematical description	Unit of M
N	Number of HPSS occurrences	$\sum_{t=1}^{T} \sum_{m=1}^{M} 1$	number
~~AvIn~~ MeanInt	Average Mean Intensity	$\frac{1}{T} \sum_{t=1}^{T} \frac{1}{M} \sum_{m=1}^{M} \texttt{tot\_tp}_m / \texttt{area}_m.$	mm/h
~~PkIn~~ PeakInt	Average Peak Intensity	$\frac{1}{T} \sum_{t=1}^{T} \frac{1}{M} \sum_{m=1}^{M} \texttt{tp\_max}_m$	mm/h
~~SpS~~ SpatExtent	~~$\frac{1}{T} \sum_{t=1}^{T} \frac{1}{M} \sum_{m=1}^{M} \texttt{axis\_maj}_m$~~ Average Maximum Linear Spatial Extent	$\frac{1}{T} \sum_{t=1}^{T} \frac{1}{M} \sum_{m=1}^{M} \texttt{max\_extent}_m$	km

~~Both AvIn and PkIn~~ Alternative metrics to N, such as the frequency of wet hours (i.e., the percentage of hours with at least one structure detected in the window), were also evaluated (Figure S1, supplementary material), with very similar patterns. However, for the sake of simplicity and to retain a more tangible indicator, the analysis is presented in terms of N rather than wet-hour frequency. Both MeanInt and PeakInt are expressed in millimetres per hour (mm/h), but they reflect different aspects of precipitation intensity. ~~AvIn~~ MeanInt represents the average intensity across all grid points of all ~~events~~ HPSSs within a given window, while ~~PkIn~~ PeakInt refers to the mean of the maximum intensities recorded at a single point for each ~~event. SpS~~ HPSS. SpatExtent indicates the average maximum linear extent of the ~~events~~ HPSSs within the same window. Finally, these values are cumulated (for N) or averaged (for ~~AvIn, PkIn, SpS~~MeanInt, PeakInt, SpatExtent) over time to obtain ~~aggregated~~ characteristic values for each location. Statistics on the full ~~event~~ dataset, including climatologies of these indicators, are presented in Section 3.1.

2.4 ~~Extreme~~ Hourly extreme precipitation ~~events~~ sub-setting

After characterising the properties of the ~~hourly precipitation events, the extremes are subset~~ HPSSs, the Hourly Precipitation Extremes (HPEs) are selected from the full ~~event~~ dataset. The selection criterion is based on the ~~average of the~~ annual maxima of hourly precipitation (RX1hour), calculated for each grid point and each year. The resulting time series of 37 RX1hour values are then averaged throughout the period 1986-2022 to derive a threshold value for each cell of the grid, representing the average RX1hour at that location. Higher threshold values were found to excessively restrict the statistical sample of extremes, whereas lower values, although expanding the subset of identified structures, would have blurred the distinction between HPEs, as defined by Extreme Value Theory (Coles, 2001), and more moderate high-quantile HPSSs, thereby reducing the interpretability of the results.

This approach is similar to the methodology used by Lavers et al. (2025), who introduced the Extreme Rain Multiplier ~~(ERM)~~ to classify extreme daily precipitation events. Lavers et al. (2025) employ ERA5 ~~, which is a global reanalysis product with a 0.25° grid spacing,~~ and consider daily precipitation accumulations to compute the mean of the annual daily maxima (RX1day). The daily accumulation is the most appropriate timescale considering the coarse spatial scale of ERA5 (Chinita

et al., 2022; Raffa et al., 2021). In contrast, this study uses a regional convection-permitting reanalysis, which provides a more accurate representation of hourly precipitation and associated extremes. Therefore, it is possible to define a threshold based on hourly maxima (RX1hour). As the last step, ~~a Gaussian filter with a 20 km radius~~ the same Gaussian filter as specified in Section 2.2 is applied to smooth the average RX1hour field and reduce local-scale noise (Figure 3).

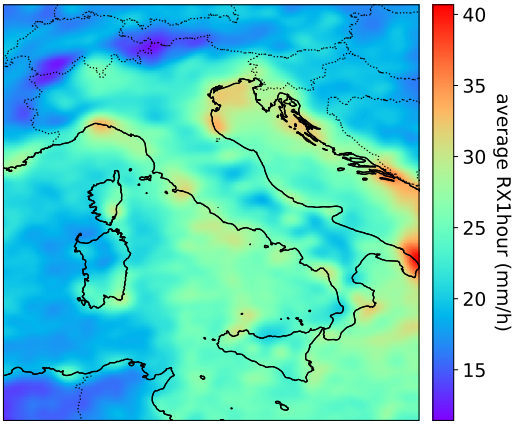

Figure 3. 1986-2022 average of the annual maxima of hourly precipitation (RX1hour), after the application of a 20 km Gaussian filter.

~~In deciding the most suitable filtering radius, several values were tested. Radii larger than 20 km excessively smooth areas with higher thresholds, reducing the ability to resolve localised extremes. Conversely, smaller radii retained too much noise, limiting the effectiveness of the filtering in isolating coherent precipitation structures. Additionally, the 20 km scale corresponds to the boundary between the meso-β and meso-γ atmospheric scales (Thunis and Bornstein, 1996), below which convective events typically occur.~~ Finally, a ~~precipitation event~~ HPSS is identified as ~~EPE~~ HPE if its maximum precipitation value (`tp_max`) exceeds the average RX1hour value in the position where it occurred (`lat_max,lon_max`). The selected HPEs can be interpreted as extreme precipitation events within a fixed-area (Eulerian) framework, which is more suitable for this study since no tracking of individual events is performed, unlike in a Lagrangian approach that follows storm structures over time (Ignaccolo and De Michele, 2010). In support of this interpretation, in section 3.3 the local persistence of HPEs is investigated, showing that HPSSs exceeding the extreme threshold are typically short-lived, rarely persisting for more than one hour, thus aligning with the common use of "extreme event" terminology.

2.5 ~~Extreme~~ Hourly Precipitation ~~Event~~ Extremes statistics and trends

Extreme statistics are calculated within the subset of ~~events classified as EPEs~~ HPSSs classified as HPEs with the same methodology described in Section 2.3. Subsequently, the trends of the yearly series of N, ~~AvIn, PkIn and SpS~~ MeanInt, PeakInt and SpatExtent are computed (results shown in Section 3.2). ~~On~~ Within each moving window, the trend analysis is performed using the Theil–Sen slope estimator (Sen, 1968), suitable for non-parametric data. The statistical significance of the trends is evaluated using the Mann–Kendall test (Mann, 1945; McLeod, 2005). To control for the multiple testing problem across the

spatial domain, the False Discovery Rate (FDR) correction is applied (Benjamini and Hochberg, 1995; Wilks, 2006). Since the FDR procedure tends to be conservative in the presence of spatial correlation, approximately correct global results can be obtained by setting the FDR threshold to twice the desired global significance level (Wilks, 2016, 2019). Therefore, results are considered statistically significant if the FDR-corrected p-value is below 0.1, corresponding to a global significance level of 0.05. The results of the trend analysis are presented in the Results section 3.3.

3 Results

3.1 ~~Full~~ Hourly precipitation ~~events dataset~~ structures analyses

~~The HOPE-X~~ Before focusing on the extremes, an analysis of the overall patterns of HPSSs across the dataset is presented, providing the necessary context for the interpretation of subsequent results on extremes. The dataset consists of approximately 160.000 precipitation ~~events~~ HPSSs per year over the period 1986-2022. The interannual variability, calculated as the relative standard deviation of the annual number of ~~events~~HPSSs, is around 10%. At the seasonal level, the highest number of ~~events~~ HPSSs is generally recorded in autumn (SON), accounting for 29% of the total, while summer (JJA) shows the lowest share, with 21%. Winter (DJF) and spring (MAM) contribute similarly, representing 26% and 24% of the total number of ~~events~~HPSSs, respectively. The fraction of hours showing no identified ~~events~~ HPSSs across the entire domain varies seasonally, with approximately 11% for winter, 12% for spring, 9% for summer, and 7% for autumn. The number of ~~events~~ HPSSs detected per hour follows ~~a distribution that decreases with increasing event count (Figure 4)~~the distribution of Figure 4.

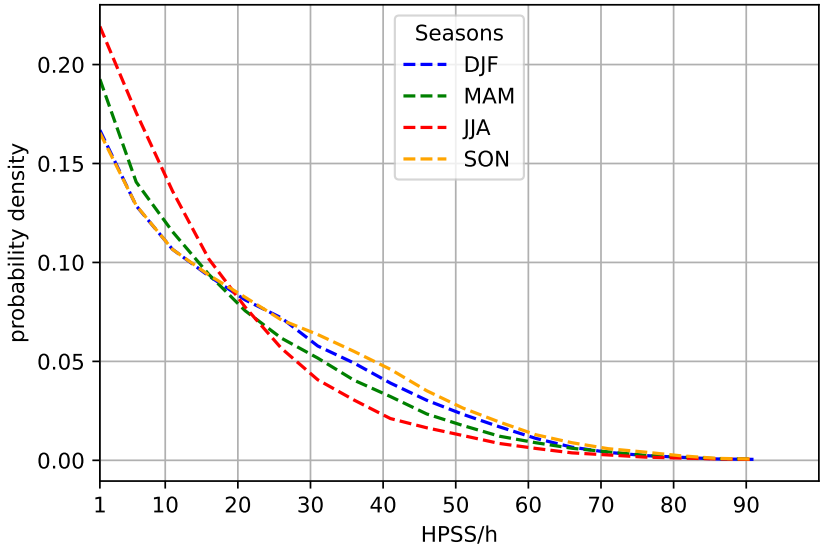

Figure 4. Distribution of the number of ~~events~~ HPSSs recorded per hour. Values are normalised by the total number of hours in each season ($24 \times 90 \times 37$). Bin width: 5.

~~Seasonal distributions of a) average intensity, b) peak intensity, and c) spatial scale of precipitation events. Bin width: 0.5 mm for intensity variables, 2 km for spatial scale. Distributions are normalised by the total number of events; that is, the sum of the integral of the four seasonal distributions gives 1.~~

The maximum number of ~~events~~ HPSSs recorded in a single hour is 136, observed at 14:00 on June 11, 1992, as a result of a widespread low-pressure area associated with large quasi-stationary cyclone influencing the whole Italian peninsula. Intensity and spatial scale distributions exhibit markedly skewed shapes, with a sharp peak at low values followed by an approximately exponential decay as their magnitude increases (Figure 5).

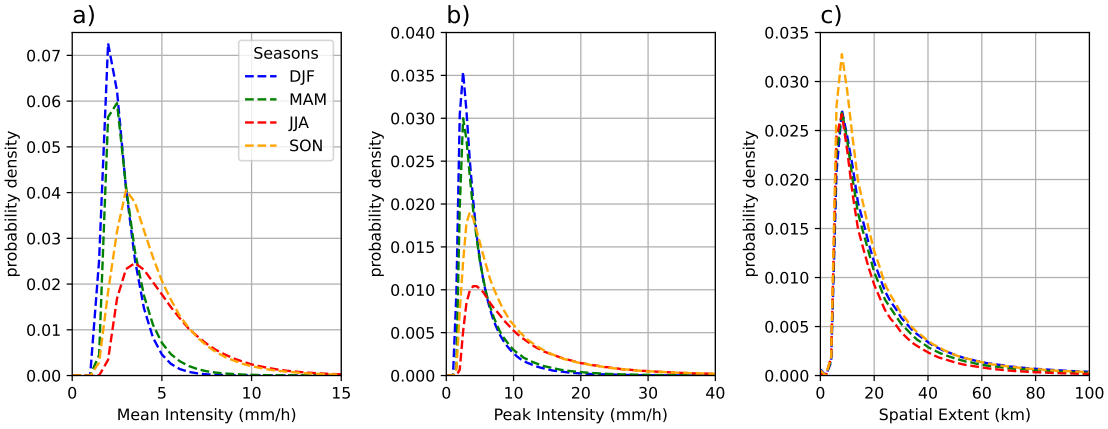

Figure 5. Seasonal distributions of a) mean intensity, b) peak intensity, and c) maximum linear spatial extent of HPSSs. Bin width: 0.5 mm for intensity variables, 2 km for spatial extent. Distributions are normalised by the total number of HPSSs; that is, the sum of the integral of the four seasonal distributions gives 1.

During summer and autumn, ~~precipitation events~~ HPSSs tend to exhibit higher median values and heavier tails for both ~~`tot_tp/area` (~~mean precipitation intensity (`tot_tp/area`, Figure 5a) and ~~`tp_max` (~~peak precipitation intensity (`tp_max`, Figure 5b). The ~~`axis_maj` (~~maximum linear spatial extent (`max_extent`, Figure 5c) distributions show less pronounced seasonal variation, with only summer displaying ~~slightly smaller-scale events~~HPSSs with a slightly smaller extent. A small percentage of ~~events~~ HPSSs fall outside the range of the distributions plotted in Figure 5: 0.22% of ~~events exhibit an~~ ~~`tot_tp/area`~~ HPSSs exhibit a mean precipitation intensity greater than 15 mm/h, 0.96% have a ~~`tp_max`~~ peak precipitation intensity above 40 mm/h, and 2.98% show a ~~`axis_maj`~~ maximum linear extent larger than 100 km. According to definitions of atmospheric scales in the scientific literature ~~(Thunis and Bornstein, 1996),~~ (Thunis and Bornstein, 1996), phenomena with lifetimes ranging from about one hour to one day—such as isolated thunderstorms or groups of storms—typically occur within the lower portion of the mesoscale, with spatial extents from approximately ~~1–~~2 km up to 200 km. ~~Our results~~ The results of HPSSs distribution analysis confirm that, at the hourly timescale, ~~significant precipitation events~~ they generally fall within the meso-γ scale (2–20 km), with only occasional instances ~~extending to larger spatial~~ exhibiting larger spatial extents. This result is consistent with the fact that precipitation structures are extracted from a 4 km convection-permitting reanalysis precipitation

field, which is capable of representing convection (Cavalleri et al., 2024a) even if it may not fully resolve it at the smaller scales. This finding is particularly relevant for applications that require knowledge of the typical spatial scales of hourly precipitation~~events~~, such as spatial analysis of precipitation fields (Fortin et al., 2018; Van Hyfte et al., 2023). ~~Moreover, it is important to note that, in this dataset, high intensities generally correspond to smaller spatial scales (see Supplementary Material, Figure S1~~In general, structures with smaller spatial extents tend to correspond to higher intensities (see supplementary material, Figure S2). Overall, the majority of ~~events~~ HPSSs concentrate on low values of intensity and ~~spatial scale~~small spatial extents. This underscores the need to isolate the most extreme ~~events~~ HPSSs to better understand their specific characteristics.

~~The results on spatial and seasonal distribution of events is~~ HPSSs are analysed using the methodology described in Section 2.3, resulting in seasonal ~~climatological means~~ maps of N (Figure 6), ~~SpS (Figure ??), AvIn (Figure ??) and PkIn (Figure ??~~SpatExtent (Figure 7), MeanInt (Figure 8) and PeakInt (not shown, see supplementary material). Higher values in a given area indicate a greater number of ~~events~~ HPSSs with their centre of mass located within that region (for N), or larger values of ~~AvIn, PkIn and SpS~~ MeanInt, PeakInt and SpatExtent for those same ~~events. Events~~ HPSSs. HPSSs may extend beyond the boundaries of the window in which they are counted, since the averaging considers only the ~~events~~ HPSSs whose centre of mass lies within the window. However, most of the recorded ~~events~~ HPSSs are well delimited in a small space (Figure 5c). It is also important to emphasise that these means are computed from distributions that are strongly right-skewed, as shown in Figure 5. Consequently, the values presented in the maps should be interpreted with some caution. While they may not fully capture the absolute characteristics of typical ~~event occurrences, scales, and intensities, they remain~~ HPSS intensity and spatial extent, they are informative when used to explore spatial and seasonal patterns and ~~relative differences across regions~~their relative differences.

The spatial distribution of N (Figure 6) shows that, in summer, most of the ~~events~~ HPSSs occur in the Prealpine regions, with secondary hotspots along parts of the Apennines, and almost no ~~events~~ HPSSs over the sea. In autumn and winter, the areas with high N shift toward coastal and offshore areas, particularly along the Tyrrhenian and Ligurian seas. During spring, the Prealps and Apennines are again prominent, although the occurrences are generally lower than in summer. The Po Valley and Prealpine region exhibit very low N ~~of events~~ during the winter season. These seasonal patterns reflect the typical climatology of convective precipitation in Italy, which tends to be more frequent during the warmer months and over mountainous regions and coastal areas (Lombardo and Bitting, 2024).

The seasonal maps of ~~SpS (Figure ??~~SpatExtent (Figure 7) reveal that during summer ~~events are generally smaller~~ HPSSs have generally smaller extents, with typical average ~~SpS~~ SpatExtent ranging between 10 and 20 km, especially along coastal areas and in southern Italy, and from 20 to 30 km in the other Italian areas. This is consistent with the convective nature of summer precipitation. ~~Springs show slightly larger SpS~~Spring shows slightly larger SpatExtent, but still below 30 km over the Prealps and in southern regions, where autumn also displays ~~those valuesof SpS~~similar values, despite showing larger ones over plain areas in the north and central Italy. In contrast, winter is characterised by generally larger ~~events~~HPSSs, especially over the Po Plain, where average ~~spatial scales~~ SpatExtent commonly reach 50 km, exceeding values registered over the

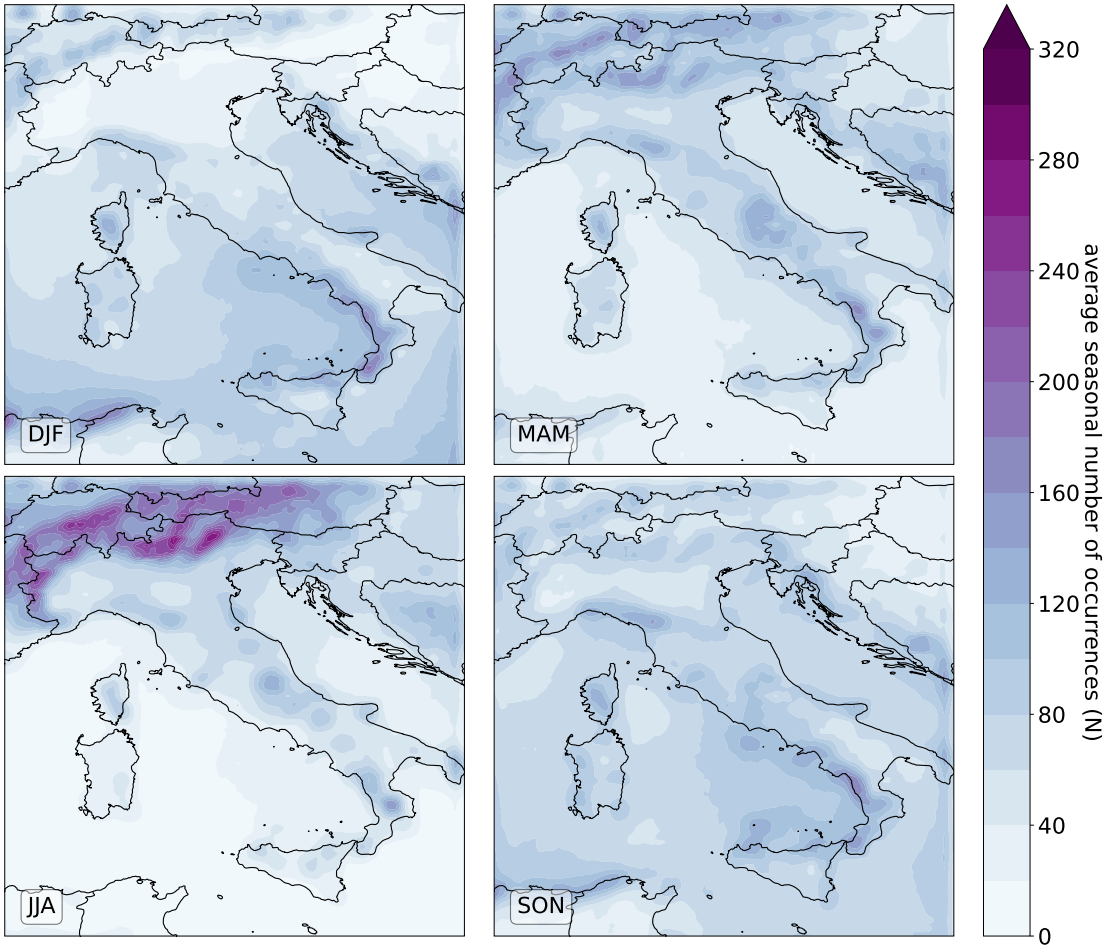

Figure 6. Seasonal map of N occurring within the 0.5 × 0.5 windows (step size 0.1), averaged over the period 1986–2022.

Alps and Apennines. This broader ~~spatial~~ extent reflects the influence of large-scale synoptic systems typical of wintertime precipitations over Italy. Overall, these patterns highlight a seasonal modulation in ~~SpS~~SpatExtent, reflecting the shift from localised convective activity in summer to more widespread, synoptic-driven precipitation in autumn and winter.

The spatial distribution of ~~AvIn (Figure ??~~MeanInt (Figure 8) highlights summer as the season with the highest average intensities, often exceeding 5 mm/h with maxima of more than 7 mm/h in some areas along the Adriatic coast, such as Calabria, the Tyrrenian sea, southeastern parts of the islands and southern Apulia. In winter, intensities generally range between 2 and 3 mm/h over most of the peninsula, dropping below 2 mm/h along the Alpine arc and exceeding this value only slightly in some southern areas and along the Tyrrhenian coast. During spring, values between 3 and 4 mm/h are widespread throughout Italy, except for isolated spots over 4 mm/h in similar areas to those observed in summer. In autumn, slightly higher intensities,

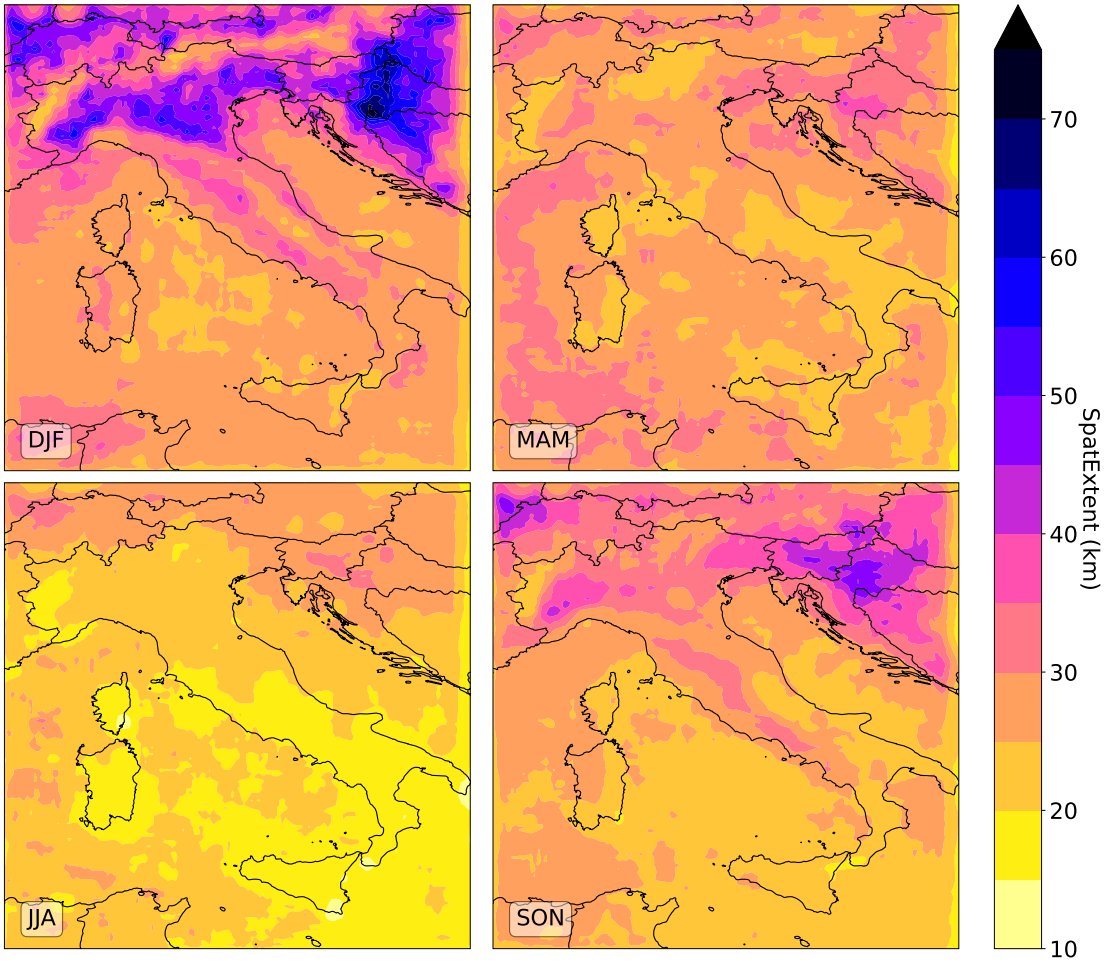

Figure 7. Seasonal map of ~~SpS~~ SpatExtent of the ~~events~~ HPSSs occurring within the 0.5 × 0.5 window (step size 0.1), averaged annually over the period 1986–2022.

ranging from 4 to 5 mm/h, cover most of the country, while lower values persist only in the Prealpine and Alpine regions. Intensities above 5 mm/h are found mainly along the coastal areas and over the surrounding seas.

~~Seasonal map of PkIn of the events occurring within the 0.5 × 0.5 window (step size 0.1), averaged annually over the period 1986–2022.~~

The ~~spatial distribution of local PkIn (Figure **??**) further emphasises the seasonal contrasts. These maps~~ seasonal patterns of PeakInt (Figure S3, supplementary material) closely resemble those for ~~AvIn, although PkIn~~ MeanInt, although PeakInt are generally higher. ~~PkIn~~ PeakInt increases from winter values ranging between 2 and 7 mm/h to well over 15 mm/h during summer, with spring and autumn showing intermediate values. Notably, in autumn, ~~PkIn~~ PeakInt exceeding 10 mm/h are

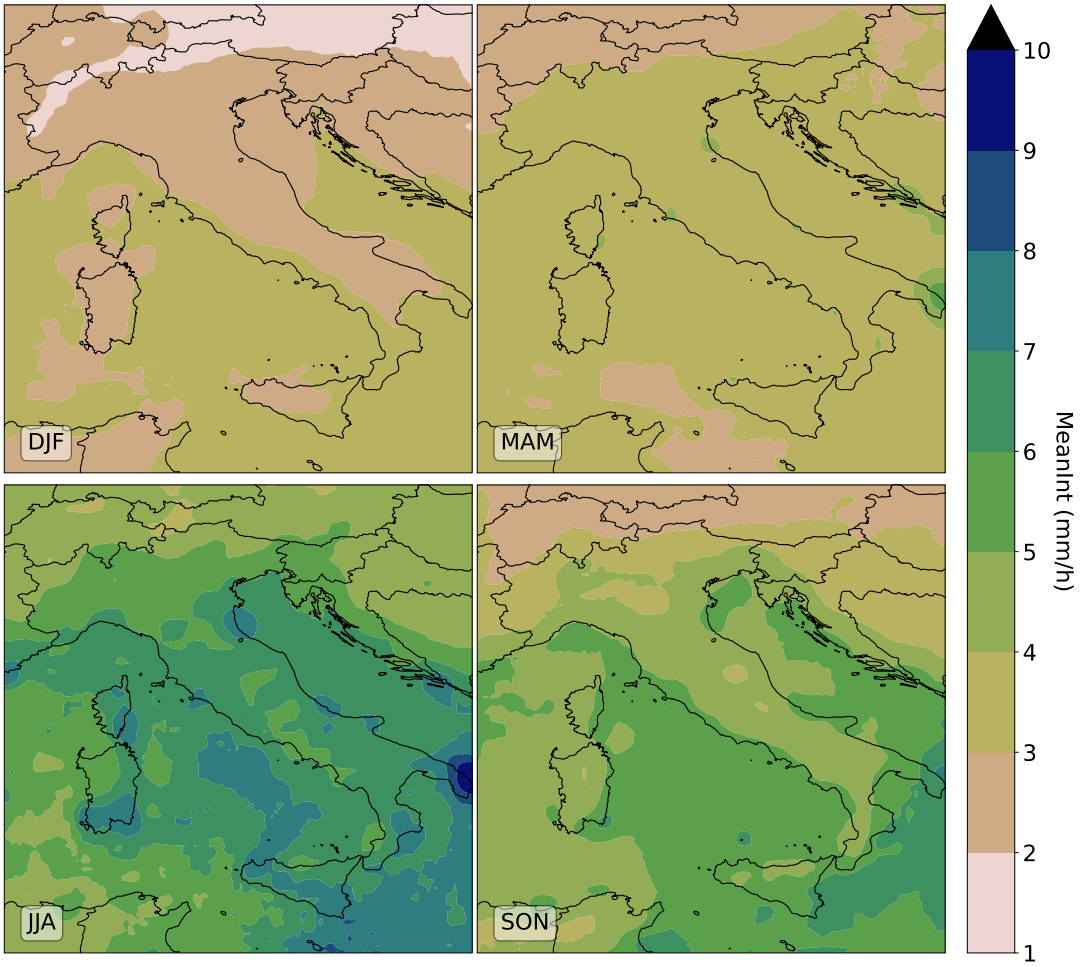

Figure 8. Seasonal map of ~~AvIn~~ MeanInt of the ~~events~~ HPSSs occurring within the 0.5 × 0.5 window (step size 0.1), averaged annually over the period 1986–2022.

mostly confined to coastal areas and the surrounding seas. In summer, ~~PkIn~~ PeakInt surpasses 17 mm/h in the same regions characterised by high summer ~~AvIn (Figure ??~~MeanInt (Figure 8).

Since it is not straightforward to determine ~~to what extent~~ the extent to which the seasonal differences in ~~Figures 6, ??, ??, and ??~~ those maps are influenced by the use of seasonally varying thresholds for ~~event~~ HPSS selection, a set of corresponding
400 figures derived from the ~~event-based~~ dataset built using a fixed 1 mm threshold is provided in the ~~Supplementary Material (Figures S2, S3, S4, and S5~~supplementary material (Figures S4-S7). These figures display very similar spatial patterns~~—~~, albeit with generally lower intensity values~~—suggesting~~ . This suggests that the observed seasonal differences primarily reflect ~~genuine variability~~ the signal of the model rather than artefacts introduced by the clustering method. Overall, ~~the climatological maps of hourly precipitation event indicators~~ these results are consistent with the established climatology of the region (Crespi

et al., 2018; Giordani et al., 2025). However, while ~~AvIn and PkIn (Figures ?? and ??)~~ MeanInt and PeakInt seasonal maps appropriately reflect higher values during the autumn and summer seasons, they also display certain inconsistencies. In particular, some areas exhibit an overrepresentation of convective activity during summer, which may not fully align with observed patterns. This issue will be examined in greater detail in the Discussion section 4.

3.2 ~~Extreme~~ Hourly Precipitation ~~Events~~ Extremes analyses

~~To gain insight into the most intense precipitation fraction, a focused analysis is conducted on a subset of EPEs, selected according to the criterion detailed in Section 2.4. The filtering procedure~~ A subset of the dataset HOPSS-X is obtained (according to Section 2.4) to gain insight into the HPEs patterns and tendencies. This resulted in approximately 4.8% ~~of all events as EPEs~~HPSSs selected as HPEs, corresponding to an average of around 7800 ~~hourly events~~ HPEs per year across the whole domain, with a notable interannual variability of about 30%. Most ~~EPEs~~ HPEs are selected from summer (11% of all summer ~~events~~HPSSs) and autumn (7%), while only a marginal fraction ~~are~~ is identified in spring (1.5%) and winter (0.5%). This seasonal breakdown results from the combined effect of higher thresholds applied for ~~event~~ HPSS identification during summer (Figure 1), which selected relatively intense ~~precipitation events~~ HPSSs even within the full dataset for that season, and the use of a fixed threshold (average RX1hour) for ~~EPE~~ HPE selection throughout the year. The greater number of ~~hourly EPEs~~ HPEs in summer and autumn is also consistent with the expectation that hourly precipitation more effectively captures extremes and their associated impacts at smaller spatial scales, such as convective storms and other meso-γ scale phenomena, particularly prevalent during the warmer seasons. Consequently, the Sections 3.2 and 3.3 focus exclusively on summer and autumn precipitation extremes.

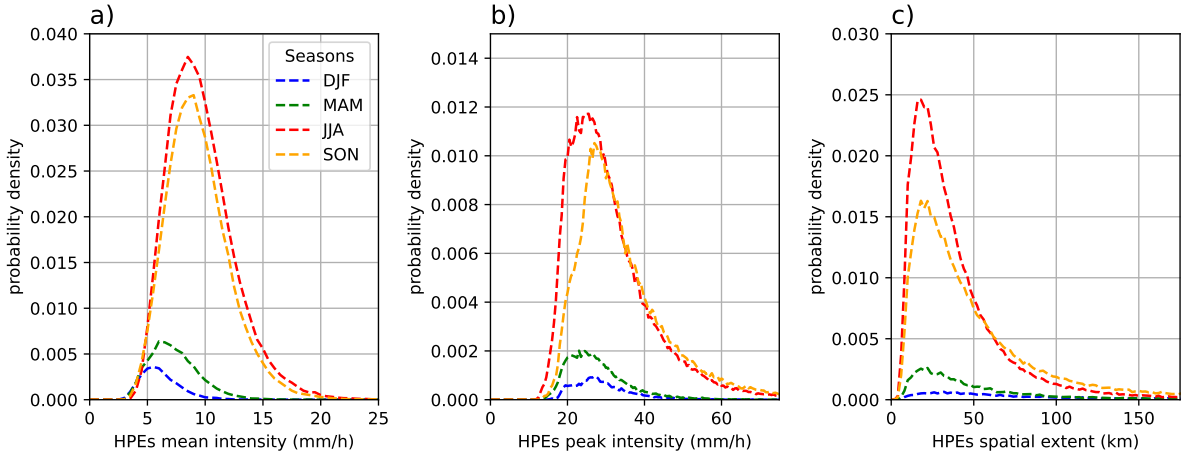

Figure 9. Seasonal distributions within the ~~EPEs~~ HPEs subset: a) ~~average~~ mean intensity, b) peak intensity, and c) maximum linear spatial ~~scale~~ extent of ~~EPEs~~HPEs. Distributions are normalised by the total number of ~~EPEs~~HPEs; that is, the sum of the integral of the four seasonal distributions gives 1. Binning as in Figure 5.

A comparison between the distributions of intensity and spatial scale within the ~~EPE~~ HPEs subset (Figure ~~??~~9) and those from the full ~~set of events~~ dataset (Figure 5) confirms that the applied filter effectively excludes a substantial number of ~~events~~ HPSSs from the lower tails of the distributions. This effect is quite obvious for the peak intensity, which is explicitly used as the filtering parameter. However, it also significantly influences the distribution of ~~average~~ mean intensity, suggesting that, on average, ~~EPEs~~ HPEs are not only more intense locally but also tend to have higher ~~average~~ mean values. Moreover, the ~~peaks of the spatial scale~~ spatial extent distributions are shifted towards larger values. Summarising, the applied filtering leads to the exclusion of a large fraction of small and weak ~~events~~HPSSs, not meaningful for the ~~EPEs~~ HPEs analysis.

The climatological seasonal maps of N within the ~~EPEs~~ HPEs subset (Figure ~~??~~10) highlights clear seasonal differences between summer and autumn.

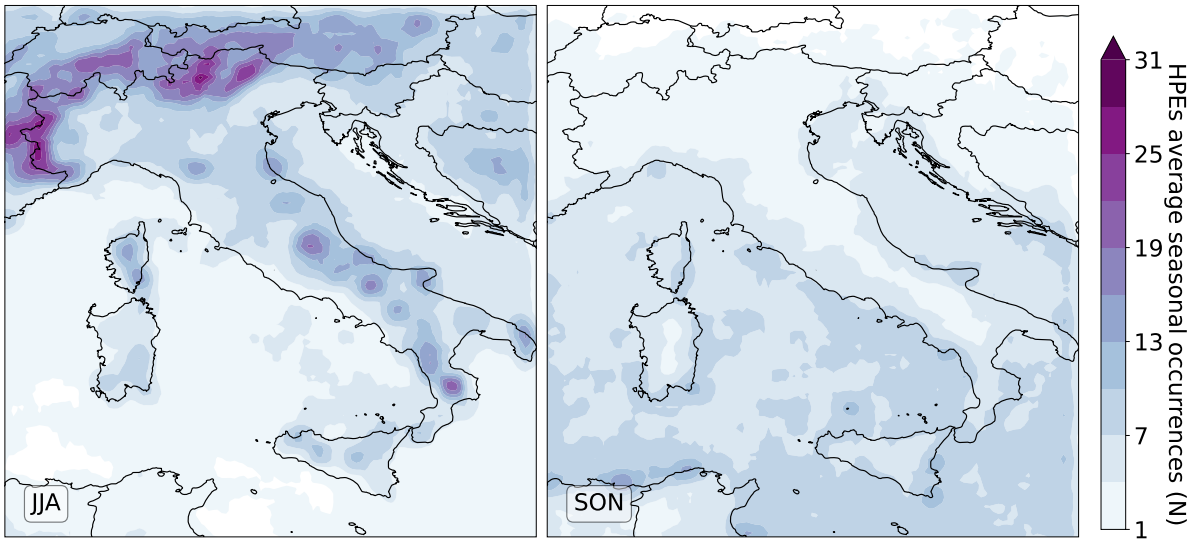

Figure 10. JJA and SON maps of ~~number~~ HPEs occurrences (N) ~~of EPEs occurring~~ within the 0.5 × 0.5 window (step size 0.1), averaged annually over the period 1986–2022.

In summer, ~~EPEs~~ HPEs occur predominantly over mountainous areas, particularly the Alps and some spots along the Apennines, and Calabria, reaching 20 to 30 ~~events~~ HPEs per 0.5° grid window per year. In contrast, coastal and marine regions display a significantly lower N, often fewer than 3 per window per year. In autumn, N is substantially less compared to summer. However, a clear spatial shift emerges: mountain areas experience fewer to none ~~events~~HPEs, while coastal and marine zones see some, with over 7 occurrences per window per year observed along many stretches of coastline. ~~This~~ The seasonal redistribution is likely driven by the persistence of ~~summer-like convective activity into early autumn at lower latitudes, where~~ warm sea surface ~~temperatures continue to support intense storm development~~ conditions beneath a cooler atmosphere, creating conditions favourable to convection and sustaining intense precipitation activity into autumn. (Cheng et al., 2022; Argüeso et al., 2024).

Marked differences between summer and autumn also emerge in terms of ~~SpS (Figure ??~~SpatExtent (Figure 11). In summer, ~~EPEs~~ HPEs rarely exceed 50 km in size, except in limited areas such as Friuli (North-East) and South Switzerland, and remain well below 20 km across much of southern Italy and the islands. Conversely, in autumn, significantly larger ~~events~~ HPEs (exceeding 100 km in spatial extent) are frequently observed. Spatial ~~scales remain smaller~~ extents remain small mainly in the south, along the Adriatic coast, and over the islands. This suggests that ~~EPEs~~ HPEs are typically small, convective systems during summer across most of the Italian territory, and during autumn along the southern coastlines. In contrast, in northern Italy and neighbouring regions, autumn ~~EPEs~~ HPEs are more frequently associated with larger-scale systems.

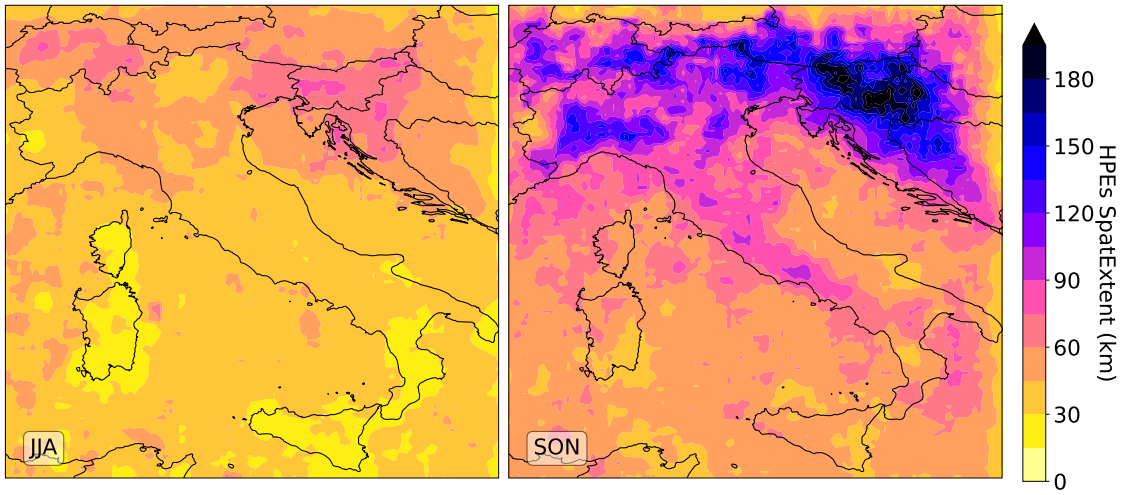

Figure 11. JJA and SON maps of ~~the Spatial Scale (SpS)~~ SpatExtent of ~~EPEs~~ the HPEs occurring within the 0.5 × 0.5 window (step size 0.1), averaged annually over the period 1986–2022.

The climatological maps for the ~~AvIn and the PkIn of EPEs~~ MeanInt and the PeakInt of HPEs are provided in the ~~Supplementary Material (Figures S6 and S7~~supplementary material (Figures S8 and S9). Overall, their spatial patterns closely resemble those observed for the full ~~set of precipitation events~~dataset, though with generally higher values, due to the filtering, which also reduces the seasonal differences. Specifically, the ~~AvIn~~ MeanInt range from approximately 5 to 15 mm/h, increasing from the Alpine regions to southern Italy for both seasons, while the ~~PkIn~~ PeakInt range from 20 up to 50 mm/h, with the lowest values again found over the Alps and the highest values concentrated in the same hotspots highlighted before, such as the southern Apulia.

3.3 ~~Extreme~~ Hourly Precipitation ~~Event~~ Extremes trends

~~Maps of the significant decadal relative trends in the number of Extreme Precipitation Events (EPEs) occurring within each 0.5° × 0.5° window (sliding step: 0.1°) for summer (JJA) and autumn (SON). Black dots indicate statistically significant trends. Areas with more than 10 years without EPEs are masked in grey. The four colored boxes for each season highlight the regions used to extract the time series shown in Figure ??.~~

~~Time series of the annual N of EPEs within the colored windows in Figure ??. The left column shows the summer (JJA) series, while the right column displays the autumn (SON) series. Trend lines are plotted for each series, and the corresponding decadal trends are reported. Grey (last row) plots denote non-significant trends.~~

Finally, given the context provided by the previous results, a trend analysis within the subset of ~~EPEs~~ HPEs is conducted, following the methodology outlined in Section 2.5. Significant trends in the number of ~~EPEs~~ HPEs occurrences (N) during summer and autumn are detected (Figure ??12). Trends are expressed as percentages relative to the seasonal and local mean values of N (i.e., normalised by the values shown in Figure ??10). For example, a 10% trend in Figure ?? 12 means a decadal increase of 10% in N, indicating that, on average in that area, approximately 30% more ~~EPEs~~ HPEs occur at the end of the study period compared to its beginning. Overall, a general increase in ~~EPEs~~ HPEs occurrences is detected across the peninsula, even though only some regions exhibit statistically significant trends.

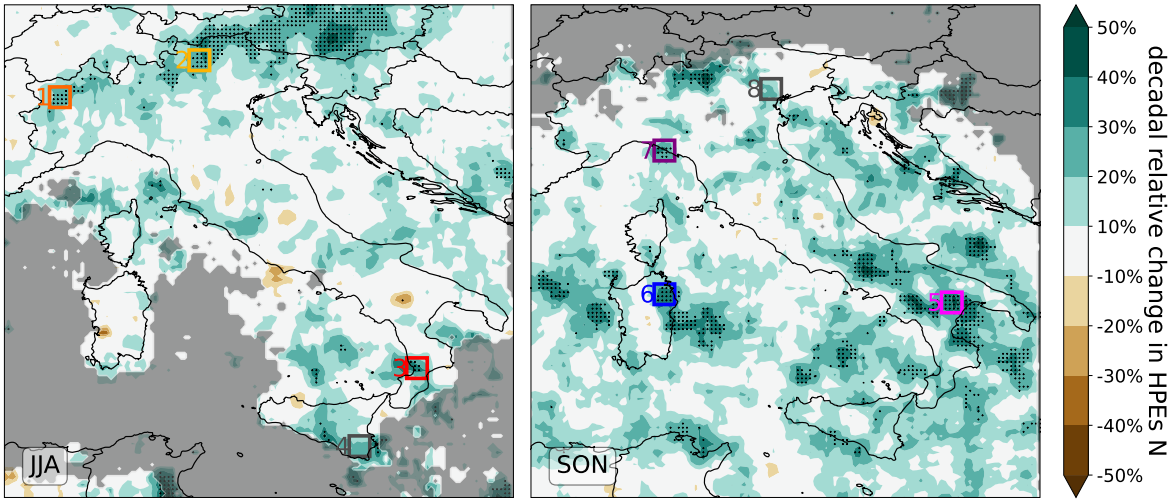

Figure 12. Maps of the significant decadal relative trends in the number of Hourly Precipitation Extremes (HPEs) occurring within each 0.5° × 0.5° window (sliding step: 0.1°) for summer (JJA) and autumn (SON). Black dots indicate statistically significant trends. Areas with more than 10 years without HPEs are masked in grey. The four colored boxes for each season highlight the regions used to extract the time series shown in Figure 13.

In summer, a significant increase of approximately 20% to 30% per decade is detected across several Alpine and Prealpine regions, and in some parts of Calabria. In autumn, significant trends are primarily concentrated over the southern Apennines, and various coastal and sea areas, such as Ligurian eastern coast, the eastern coast of Sardinia, the southern Adriatic Sea, and the Ionian Sea. Individual series of some selected areas (specifically, inside ~~coloured~~ colored 0.5 degree ~~windows of Figure ??~~boxes of Figure 12) are extracted to visualise the ~~EPEs N series~~ HPEs annual occurrences along with the detected trends (Figure ??13). In summer, trends ranging from 10% to 40%, depending on the region, correspond to an increase of 2 to 6 ~~extreme precipitation events (EPEs)~~ HPEs per decade. In autumn, comparable percentage changes are associated with

a smaller increase of 1 to 2 ~~EPEs~~ HPEs per decade. In both seasons, some regions also display positive trends that are not statistically significant (e.g., ~~Boxes~~ boxes 4 and 8 in ~~Figure ??~~Figures 12 and 13), likely due to high interannual variability that dominates the signal.

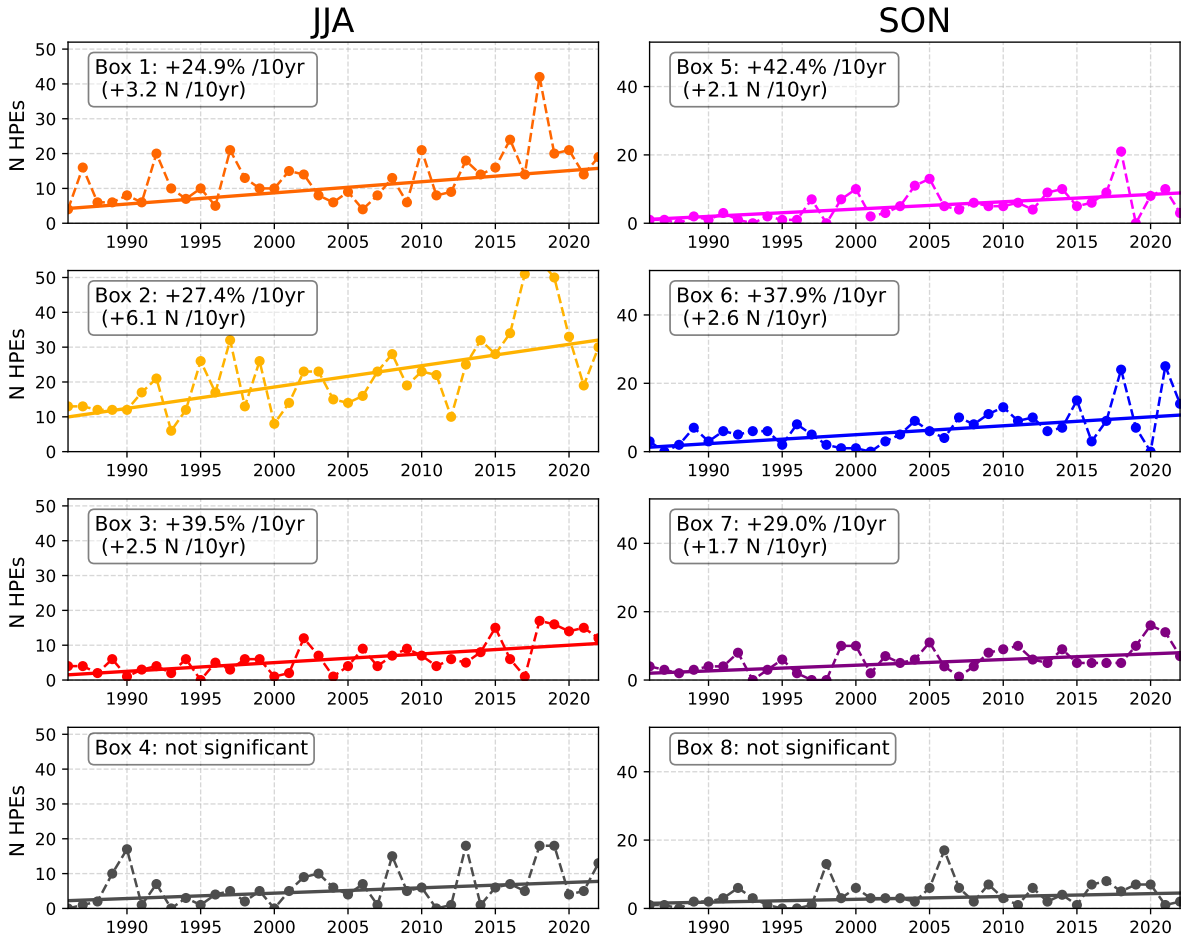

Figure 13. Time series of the annual N of HPEs within the colored windows in Figure 12. The left column shows the summer (JJA) series, while the right column displays the autumn (SON) series. Trend lines are plotted for each series, and the corresponding decadal trends are reported. Grey (last row) plots denote non-significant trends.

480 Trends are also computed for the ~~SpS, AvIn, and PkIn of EPEs (see Supplementary~~ SpatExtent, MeanInt, and PeakInt of HPEs (see supplementary material, Figures ~~S8, S9, S10~~S10, S11, S12, respectively). Overall, only weak trends (below 10%~~a decadeover Italy~~/decade) are observed, primarily over land points in summer and over some marine areas in autumn, showing ~~alternating patterns~~ spatial heterogeneity in the sign of the signal with a slight tendency toward increasing intensities and decreasing spatial scales. However, none of these trends is statistically significant at any location. This suggests that changes

485 over time are more likely associated with the frequency of ~~EPEs~~ HPEs rather than their intensity or spatial extent. It may also reflect the lower noise sensitivity of ~~event counts~~ N compared to other indicators. ~~Moreover, trend estimates based on N~~

Trend estimates could be biased by potential double-counting of temporally persistent ~~events~~HPEs, as the analysis is conducted at hourly resolution. To address this, an additional analysis quantifies ~~event~~ HPEs persistence, defined as the number of consecutive hours during which an ~~EPE (i.e., an event exceeding~~ HPSS exceeds the local average RX1hour threshold ~~) affects~~
490 within the same window.

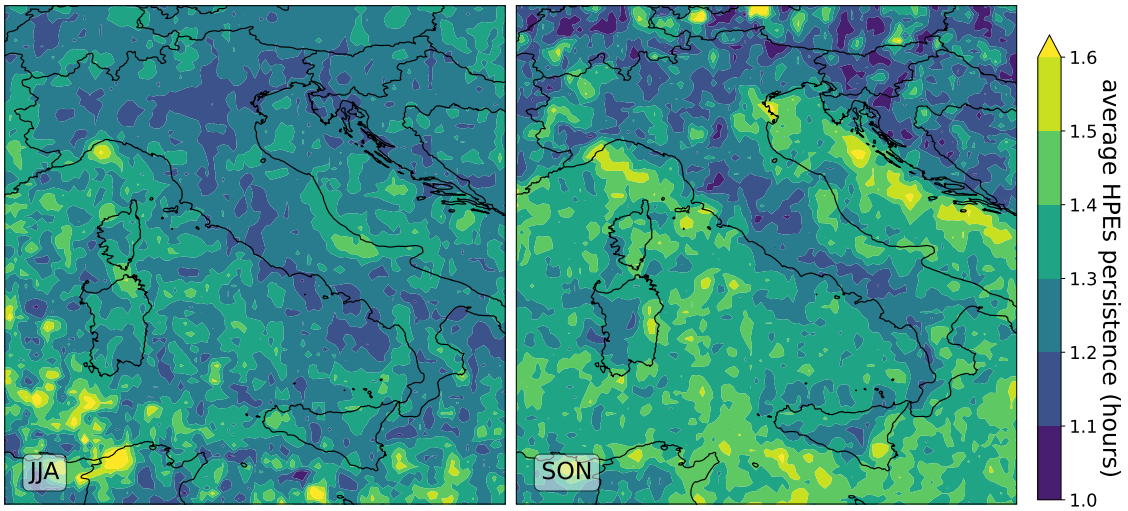

Figure 14. seasonal (JJA and SON) maps of the average ~~EPEs~~ HPEs persistence (expressed in hours) occurring within the 0.5 × 0.5 window (step size 0.1).

Results (Figure ~~??~~14) show that persistence exceeds one hour only marginally in most regions, with average persistence values above 1.5 hours limited to a few localised areas expecially during autumn, such as the Ligurian Gulf, where persistent mesoscale convective systems are more common (Cassola et al., 2016), and in parts of eastern Sardinia and southeastern Sicily, where prolonged convective activity can occur (Forestieri et al., 2018). These findings support the overall temporal isolation of
495 most ~~EPEs~~ HPEs and suggest that the impact of double-counting on trend estimates remains limited.

4 Discussion

In understanding the results of this work, it is important to underline the uncertainties in analysing signals from ~~the reanalysis representation of hourly precipitation . The MERIDA HRESreanalysis provides hourly precipitation fields over a continuous and homogeneous 37-year period; however, some limitations affect MERIDA HRES, particularly concerning the representation~~
500 ~~of precipitation fields at the~~ hourly ~~scale. While the temporal stability and spatial accuracy of MERIDA HRES have been verified in previous studies from climatological to hourly timescales (Cavalleri et al., 2024a; Giordani et al., 2025), it is still~~

~~necessary to discuss some potential inconsistencies and their impact on the results of this work. Specifically, previous studies have shown that MERIDA HRES systematically overestimates rainfall in summer (and partly in autumn) in regions like the Po Valley–Adriatic interface, the Calabrian mountains, southern Apulia, and southeastern islands (Cavalleri et al., 2024a; Viterbo et al., 2024; C~~

505 precipitation as represented by MERIDA HRES. First, while this 4 km model can explicitly represent convective processes (Viterbo et al., 2024; Cavalleri et al., 2024a), it may not fully resolve all aspects of these phenomena. For the purposes of this study, however, the HPSS isolated from MERIDA HRES hourly fields resulted consistent with the spatial scales under investigation (Thunis and Bornstein, 1996) and allows for a characterization of hourly precipitation patterns, even if some sub-grid aspects of convection may not be fully captured.

510 Then, as described in Section 2.1, a precipitation overestimation bias is present in summer. These localised wet biases ~~, consistent across timescales, likely stem from~~ are likely due to overly active explicit convection in the model, as ~~suggested by Figure ?? and ??~~shown in Figure 8. This behaviour ~~is sometimes common in WRF-based dynamical downscalings of ERA5 (Bernini et al., 2025), due to some possible problems in representing skin temperature , and difficulty capturing complex~~ may be associated with a less accurate estimation of skin temperature at the land-sea ~~interactions that often arise~~ interface

515 due to the interpolation of skin temperature from the coarse ERA5 domain to the finer-resolution MERIDA HRES domain. Overestimation of skin temperature may occur at certain points along the coastlines, leading to high values of latent heat flux. In particular meteorological conditions associated with convective instability, this may exacerbate convection, resulting in an overestimation of precipitation ~~in areas where it is not normally observed. Even if these aspects need to be taken into account~~amounts.

520 However, it is important to notice that these biases are temporally stable and do not coincide spatially with the areas showing significant ~~EPEs increases. Moreover, it is important to underline that ERA5 (Lussana et al., 2024) and its regional downscalings (Cavalleri et al., 2024a) can exhibit stronger precipitation trends than the observed ones. In particular, Cavalleri et al. (2024a) highlighted that the trend in the differences between MERIDA HRES and homogenised observations annual precipitation totals is about~~ HPSs increases. Another aspect to consider is the deviation of MERIDA HRES annual precipitation trends

525 from observational ones (Cavalleri et al., 2024a). The average deviation over Italy has been quantified at approximately 4% for decade~~, meaning that this fraction of annual precipitation increase might be attributable to a deviation from observations rather than a true climate signal~~. This value is not negligible, but ~~overall~~ relatively small if compared to the 10% to 40% increases found in ~~EPEs occurrences. Even with respect to this additional inhomogeneity, the areas affected by it, as delineated in the~~ HPEs occurrences. Moreover, the regions where this discrepancy is more marked (see supplementary material of Cavalleri

530 et al. (2024a)~~,~~) do not overlap with those in which significant trends in ~~EPEs~~ HPEs occurrences have been found. In principle, such biases could have masked decreasing trends in those areas; however, the overall spatial pattern suggests that this scenario is highly unlikely.

The increasing trends in hourly ~~EPEs~~ HPEs identified in this study for the period 1986–2022 align with several previous

535 research efforts based on both sub-daily and daily extreme precipitation observations across Italy and its specific regions. In

particular, Mazzoglio et al. (2025) reported positive trends in the same Prealpine area analyzed here, based on the RX1hour index, largely attributed to summer convective activity. At a regional scale, Dallan et al. (2022) examined extreme precipitation trends from 1991 to 2020 by separating storm intensity and occurrence frequency, attributing the observed increases in the Eastern Alps to a growing proportion of sub-daily convective storms during summer. Similarly, Persiano et al. (2020) found a generalized increase in both the frequency and intensity of sub-daily extreme rainfall over the Apennines in Emilia-Romagna (northern Italy) for the 1961–2015 period. Moreover, Pavan et al. (2019), using a daily gridded precipitation dataset for the north and central Italy covering 1961–2015, reported significant positive trends in the 90th percentile of daily precipitation across most of the Alpine area and the northern Po Valley during summer, also supporting the idea that summer and autumn are the seasons most affected by precipitation changes. In autumn, some of the hourly ~~EPEs~~ HPEs trends detected in this study agree with findings by Capozzi et al. (2023), who, based on daily station data for the 2002–2021 period, documented an increasing tendency in both the intensity and frequency of heavy rainfall events in inland Campania. Additionally, the autumnal trends over the central ~~Pre-Alps~~ Prealps are in line with the results of Pavan et al. (2019), who also reported significant increases in daily precipitation extremes over the Alps during autumn. This kind of local evidence provides an important observational context that supports the reliability of some of the signals identified through the present reanalysis-based approach.

5 Conclusions

This study employs hourly precipitation fields from the convection-permitting MERIDA-HRES reanalysis to investigate the characteristics of hourly precipitation ~~events~~spatial structures, with a focus on ~~their most extreme components~~ the extremes and their temporal evolution over the period 1986–2022. This approach yields a twofold outcome. First, it enables the construction of the ~~HOPE-X~~ HOPSS-X dataset, an ~~event-based~~ archive in which nearly 6 million ~~significant precipitation events~~ precipitation structures are described by a set of intensity and spatial characteristics. Second, ~~by isolating the most extreme subset of these events, the method facilitates~~ a method is proposed to facilitate the description of ~~extreme patterns and the detection of~~ hourly precipitation patterns, and, by isolating the most extreme subset, to detect statistically significant trends in the occurrence of ~~EPEs during summer and autumn~~hourly extremes.

In summer, increasing trends in HPEs occurrences are detected over several Alpine and Prealpine regions as well as in parts of Calabria. In autumn, the most prominent trends emerged over the southern Apennines, over the central ~~Pre-Alps~~Prealps, and several maritime regions, including Ligurian eastern coast, the eastern coast of Sardinia, the southern Adriatic Sea, and the Ionian Sea.

The results obtained in this work represent an additional perspective within the ongoing and complex debate on precipitation trends in Italy, even with full awareness of some of the limitations of reanalysis datasets. Spatial uncertainty of MERIDA HRES reanalysis was addressed through ~~an event-based~~ a structure-based approach, which allowed the identification and subsequent spatial aggregation of ~~hourly events~~ HPSSs using moving windows, with the intent of reducing the impact of spatial

misplacement errors. The results were also interpreted in light of some known and documented local biases of the reanalysis, such as the systematic -thought constant- overestimation of convective precipitation in some areas and ~~some discrepancies~~ local deviations between modelled and observed trends at longer timescales. ~~In the final results, regions affected by these model biases were carefully considered in the interpretation of the results and generally did not overlap with the~~ The areas where statistically significant trends in the occurrence of ~~EPEs were detected .~~

HPEs are detected generally did not overlap with these of such inconsistencies, supporting the robustness of the results.

The comparison with previous works on precipitation trends and extremes, based on observational data at both daily and sub-daily timescales, supports the robustness of the results presented in this work. In particular, the consistency observed across different studies strengthens the evidence of increasing occurrences of ~~hourly EPEs~~ HPEs over specific regions of Italy during summer and autumn.

Future developments may involve leveraging the ~~event-based dataset HOPE-X~~ dataset HOPSS-X to explore additional characteristics of ~~EPEs~~hourly precipitation structures, such as their dominant propagation direction and potential associations with changes in large-scale atmospheric circulation (Iacomino et al., 2025). In selected regions, identifying and employing sufficiently long hourly observational records could allow for a more direct validation of the detected trends. The approach could also be extended to identify ~~EPEs~~ precipitation structures of different nature and duration, including synoptic-scale ~~events~~precipitation structures, by analysing longer accumulation periods (e.g., 3, 6, 12, or 24 hours). Furthermore, similar ~~event-based datasets~~ datasets based on precipitation structures could be produced using the same methodology to detect ~~EPEs~~ precipitation extremes in other regions where convection-permitting reanalyses are available.

Code and data availability. MERIDA-HRES data are openly available from the RSE repository: "PREC" at https://merida.rse-web.it/. The HPSSs dataset used and produced in this study is openly available on Zenodo (DOI: 10.5281/zenodo.15772543), or via the short link https://bit.ly/HOPSS-X. The code used in this work is openly available on GitHub: https://github.com/fcavalleri/HPEs.git.

Author contributions. FC: Conceptualization; Formal Analysis; Investigation; Software; Visualization; Writing – Original Draft Preparation; CL: Conceptualization; Methodology; Investigation; Supervision; Validation; Writing – Review & Editing; FV: Data Curation; Methodology; Investigation; Supervision; Validation; Writing – Review & Editing; MB: Investigation; Writing – Review & Editing; RB: Data Curation; Investigation; Writing – Review & Editing; VM: Investigation; Writing – Review & Editing; ML: Data Curation; Investigation; Funding Acquisition; Writing – Review & Editing; MM: Investigation; Supervision; Validation; Writing – Review & Editing; Funding Acquisition.

Competing interests. The authors declare that they have no known competing financial interests or personal relationships that could have appeared to influence the work reported in this paper.

Acknowledgements. The PhD of the co-author Francesco Cavalleri was activated pursuant to DM 352 and is co-sponsored by PNRR funds and R.S.E. s.p.a. The PNRR funds come from the EU Next Generation programme. This work has been financed by the Research Fund for the Italian Electrical System under the Three-Year Research Plan 2025-2027 (MASE, Decree n.388 of November 6th, 2024), in compliance with the Decree of April 12th, 2024. This work has been financed by Research Funds from the Italian Ministry for University and Research (PRIN 2022 - CN4RWK – CCHP-ALPS – Climate Change and HydroPower in the Alps, funded by the European Union (Programme Next Generation EU)). Veronica Manara was supported by the "Ministero dell'Università e della Ricerca" of Italy [grant FSE – REACT EU, DM 10/08/2021 n. 1062].

During the preparation of this work, the authors used ChatGPT in order to enhance readability. After using this tool, the authors reviewed and edited the content as needed and take full responsibility for the content of the publication.

References

Allan, R. P., Barlow, M., Byrne, M. P., Cherchi, A., Douville, H., Fowler, H. J., Gan, T. Y., Pendergrass, A. G., Rosenfeld, D., Swann, A. L. S., Wilcox, L. J., and Zolina, O.: Advances in understanding large-scale responses of the water cycle to climate change, Annals of the New York Academy of Sciences, 1472, 49–75, https://doi.org/https://doi.org/10.1111/nyas.14337, 2020.

Argüeso, D., Marcos, M., and Amores, A.: Storm Daniel fueled by anomalously high sea surface temperatures in the Mediterranean, npj Climate and Atmospheric Science, https://doi.org/10.1038/s41612-024-00872-2, 2024.

Avino, A., Cimorelli, L., Furcolo, P., Noto, L. V., Pelosi, A., Pianese, D., Villani, P., and Manfreda, S.: Are rainfall extremes increasing in southern Italy?, Journal of Hydrology, 631, 130 684, 2024.

Bartolini, G., Messeri, A., Grifoni, D., Mannini, D., and Orlandini, S.: Recent trends in seasonal and annual precipitation indices in Tuscany (Italy), Theoretical and applied climatology, 118, 147–157, 2014.

Benjamini, Y. and Hochberg, Y.: Controlling the false discovery rate: a practical and powerful approach to multiple testing, Journal of the Royal statistical society: series B (Methodological), 57, 289–300, 1995.

Bernini, L., Lagasio, M., Milelli, M., Oberto, E., Parodi, A., Hachinger, S., Kranzlmüller, D., and Tartaglione, N.: Convection-permitting dynamical downscaling of ERA5 for Europe and the Mediterranean basin, Quarterly Journal of the Royal Meteorological Society, p. e5014, 2025.

Blenkinsop, S., Fowler, H. J., Barbero, R., Chan, S. C., Guerreiro, S. B., Kendon, E., Lenderink, G., Lewis, E., Li, X.-F., Westra, S., Alexander, L., Allan, R. P., Berg, P., Dunn, R. J. H., Ekström, M., Evans, J. P., Holland, G., Jones, R., Kjellström, E., Klein-Tank, A., Lettenmaier, D., Mishra, V., Prein, A. F., Sheffield, J., and Tye, M. R.: The INTENSE project: using observations and models to understand the past, present and future of sub-daily rainfall extremes, Advances in Science and Research, 15, 117–126, https://doi.org/10.5194/asr-15-117-2018, 2018.

Bonanno, R., Lacavalla, M., and Sperati, S.: A new high-resolution MEteorological Reanalysis Italian DAtaset: MERIDA, Quarterly Journal of the Royal Meteorological Society, 145, 1756–1779, https://doi.org/https://doi.org/10.1002/qj.3530, 2019.

Brugnara, Y., Brunetti, M., Maugeri, M., Nanni, T., and Simolo, C.: High-resolution analysis of daily precipitation trends in the central Alps over the last century., International Journal of Climatology, 32, 2012.

Brunetti, M., Caloiero, T., Coscarelli, R., Gullà, G., Nanni, T., and Simolo, C.: Precipitation variability and change in the Calabria region (Italy) from a high resolution daily dataset, International Journal of Climatology, 32, 57, 2012.

Caloiero, T., Caloiero, P., and Frustaci, F.: Long-term precipitation trend analysis in Europe and in the Mediterranean basin, Water and Environment Journal, 32, 433–445, 2018.

Caloiero, T., Coscarelli, R., and Pellicone, G.: Trend analysis of rainfall using gridded data over a region of southern Italy, Water, 13, 2271, 2021.

Capecchi, V., Pasi, F., Gozzini, B., and Brandini, C.: A convection-permitting and limited-area model hindcast driven by ERA5 data: precipitation performances in Italy, Climate Dynamics, 61, 1411–1437, https://doi.org/doi.org/10.1007/s00382-022-06633-2, 2023.

Capozzi, V., Rocco, A., Annella, C., Cretella, V., Fusco, G., and Budillon, G.: Signals of change in the Campania region rainfall regime: An analysis of extreme precipitation indices (2002–2021), Meteorological Applications, 30, e2168, 2023.

Cassola, F., Ferrari, F., Mazzino, A., and Miglietta, M.: The role of the sea on the flash floods events over Liguria (northwestern Italy), Geophysical Research Letters, 43, 3534 – 3542, https://doi.org/10.1002/2016GL068265, 2016.

Cavalleri, F., Lussana, C., Viterbo, F., Brunetti, M., Bonanno, R., Manara, V., Lacavalla, M., Sperati, S., Raffa, M., Capecchi, V., et al.: Multi-scale assessment of high-resolution reanalysis precipitation fields over Italy, Atmospheric Research, 312, 107 734, 2024a.

Cavalleri, F., Viterbo, F., Brunetti, M., Bonanno, R., Manara, V., Lussana, C., Lacavalla, M., and Maugeri, M.: Inter-comparison and validation of high-resolution surface air temperature reanalysis fields over Italy, International Journal of Climatology, 44, 2681–2700, https://doi.org/https://doi.org/10.1002/joc.8475, 2024b.

Cerenzia, I. M. L., Giordani, A., Paccagnella, T., and Montani, A.: Towards a convection-permitting regional reanalysis over the Italian domain, Meteorological Applications, 29, e2092, https://doi.org/https://doi.org/10.1002/met.2092, 2022.

Chang, W., Stein, M. L., Wang, J., Kotamarthi, V. R., and Moyer, E. J.: Changes in spatiotemporal precipitation patterns in changing climate conditions, Journal of Climate, 29, 8355–8376, 2016.

Cheng, K., Harris, L., Bretherton, C., Merlis, T., Bolot, M., Zhou, L., Kaltenbaugh, A., Clark, S. K., and Fueglistaler, S.: Impact of Warmer Sea Surface Temperature on the Global Pattern of Intense Convection: Insights From a Global Storm Resolving Model, Geophysical Research Letters, 49, https://doi.org/10.1029/2022GL099796, 2022.

Chinita, M. J., Witte, M., Kurowski, M. J., Teixeira, J., Suselj, K., Matheou, G., and Bogenschutz, P.: Improving the representation of shallow cumulus convection with the Simplified Higher-Order Closure Mass-Flux (SHOC+ MF v1. 0) approach, Geoscientific Model Development Discussions, 2022, 1–23, 2022.

Coles, S.: An Introduction to Statistical Modeling of Extreme Values, Springer-Verlag, London, https://doi.org/10.1007/978-1-4471-3675-0, 2001.

Crespi, A., Brunetti, M., Lentini, G., and Maugeri, M.: 1961–1990 high-resolution monthly precipitation climatologies for Italy, International Journal of Climatology, 38, 878–895, https://doi.org/https://doi.org/10.1002/joc.5217, 2018.

Dallan, E., Borga, M., Zaramella, M., and Marra, F.: Enhanced Summer Convection Explains Observed Trends in Extreme Subdaily Precipitation in the Eastern Italian Alps, Geophysical Research Letters, 49, e2021GL096 727, https://doi.org/https://doi.org/10.1029/2021GL096727, 2022.

Dallan, E., Borga, M., Fosser, G., Canale, A., Roghani, B., Marani, M., and Marra, F.: A Method to Assess and Explain Changes in Sub-Daily Precipitation Return Levels from Convection-Permitting Simulations, Water Resources Research, 60, e2023WR035 969, https://doi.org/10.1029/2023WR035969, 2024.

Davis, C., Brown, B., and Bullock, R.: Object-based verification of precipitation forecasts. Part II: Application to convective rain systems, Monthly Weather Review, 134, 1785–1795, 2006.

Donat, M. G., Lowry, A. L., Alexander, L. V., et al.: Addendum: More extreme precipitation in the world's dry and wet regions, Nature Climate Change, 7, 154–158, https://doi.org/https://doi.org/10.1038/nclimate3160, 2017.

Donnini, M., Santangelo, M., Gariano, S. L., Bucci, F., Peruccacci, S., Alvioli, M., Althuwaynee, O., Ardizzone, F., Bianchi, C., Bornaetxea, T., et al.: Landslides triggered by an extraordinary rainfall event in Central Italy on September 15, 2022, Landslides, 20, 2199–2211, 2023.

Fantini, A.: Climate Change Impact on Flood Hazard Over Italy, Ph.D. thesis, Università degli Studi di Trieste, https://arts.units.it/handle/11368/2940009, phD Thesis, 2019.

Forestieri, A., Arnone, E., Blenkinsop, S., Candela, A., Fowler, H., and Noto, L. V.: The impact of climate change on extreme precipitation in Sicily, Italy, Hydrological Processes, 32, 332–348, https://doi.org/https://doi.org/10.1002/hyp.11421, 2018.

Fortin, V., Roy, G., Stadnyk, T., Koenig, K., Gasset, N., and and, A. M.: Ten Years of Science Based on the Canadian Precipitation Analysis: A CaPA System Overview and Literature Review†, Atmosphere-Ocean, 56, 178–196, https://doi.org/10.1080/07055900.2018.1474728, 2018.

Fowler, H. J., Lenderink, G., Prein, A. F., Westra, S., Allan, R. P., Ban, N., Barbero, R., Berg, P., Blenkinsop, S., Do, H. X., Guerreiro, S., Haerter, J. O., Kendon, E. J., Lewis, E., Schaer, C., Sharma, A., Villarini, G., Wasko, C., and Zhang, X.: Anthropogenic intensification of short-duration rainfall extremes, Nature Reviews Earth & Environment, 2, 107–122, https://doi.org/10.1038/s43017-020-00128-6, 2021.

Garcia-Soto, C., Cheng, L., Caesar, L., Schmidtko, S., Jewett, E. B., Cheripka, A., Rigor, I., Caballero, A., Chiba, S., Báez, J. C., Zielinski, T., and Abraham, J. P.: An Overview of Ocean Climate Change Indicators: Sea Surface Temperature, Ocean Heat Content, Ocean pH, Dissolved Oxygen Concentration, Arctic Sea Ice Extent, Thickness and Volume, Sea Level and Strength of the AMOC (Atlantic Meridional Overturning Circulation), Frontiers in Marine Science, 8, 642 372, https://doi.org/10.3389/fmars.2021.642372, 2021.

Giordani, A., Cerenzia, I. M. L., Paccagnella, T., and Di Sabatino, S.: SPHERA, a new convection-permitting regional reanalysis over Italy: Improving the description of heavy rainfall, Quarterly Journal of the Royal Meteorological Society, 149, 781–808, https://doi.org/https://doi.org/10.1002/qj.4428, 2023.

Giordani, A., Ruggieri, P., and Di Sabatino, S.: Added Value of a Multi-Model Ensemble of Convection-Permitting Rainfall Reanalyses Over Italy, https://doi.org/10.2139/ssrn.5227549, preprint, 2025.

Giovannini, L., Davolio, S., Zaramella, M., Zardi, D., and Borga, M.: Multi-model convection-resolving simulations of the October 2018 Vaia storm over Northeastern Italy, Atmospheric Research, 253, 105 455, 2021.

Hardwick Jones, R., Westra, S., and Sharma, A.: Observed Relationships between Extreme Sub-Daily Precipitation, Surface Temperature, and Relative Humidity, Geophysical Research Letters, 37, L22 805, https://doi.org/10.1029/2010GL045081, 2010.

Hersbach, H., Bell, B., Berrisford, P., Hirahara, S., Horanyi, A., Munoz-Sabater, J., Nicolas, J., Peubey, C., Radu, R., Schepers, D., Simmons, A., Soci, C., Abdalla, S., Abellan, X., Balsamo, G., Bechtold, P., Biavati, G., Bidlot, J., Bonavita, M., Chiara, G., Dahlgren, P., Dee, D., Diamantakis, M., Dragani, R., Flemming, J., Forbes, R., Fuentes, M., Geer, A., Haimberger, L., Healy, S., Hogan, R. J., Holm, E., Janiskova, M., Keeley, S., Laloyaux, P., Lopez, P., Lupu, C., Radnoti, G., Rosnay, P., Rozum, I., Vamborg, F., Villaume, S., and Thepaut, J.: The ERA5 global reanalysis, Quarterly Journal of the Royal Meteorological Society, 146, 1999–2049, https://doi.org/10.1002/qj.3803, 2020.

Hohenegger, C. and Schär, C.: Predictability and Error Growth Dynamics in Cloud-Resolving Models, Journal of the Atmospheric Sciences, 64, 4467 – 4478, https://doi.org/10.1175/2007JAS2143.1, 2007.

Iacomino, C., Pascale, S., Zappa, G., Iotti, M., Grazzini, F., Ghinassi, P., and Portal, A.: A Classification of High-Risk Atmospheric Circulation Patterns for Italian Precipitation Extremes, International Journal of Climatology, p. e70118, https://doi.org/https://doi.org/10.1002/joc.70118, 2025.

Ignaccolo, M. and De Michele, C.: A point based Eulerian definition of rain event based on statistical properties of inter drop time intervals: An application to Chilbolton data, Advances in Water Resources, 33, 933–941, https://doi.org/https://doi.org/10.1016/j.advwatres.2010.04.002, 2010.

IPCC: Climate Change 2021 – The Physical Science Basis: Working Group I Contribution to the Sixth Assessment Report of the Intergovernmental Panel on Climate Change, Cambridge University Press, https://doi.org/10.1017/9781009157896, 2023.

Kalnay, E., Mote, S., and Da, C.: Earth System Modeling, Data Assimilation and Predictability: Atmosphere, Oceans, Land and Human Systems, Cambridge University Press, 2 edn., 2024.

Lavers, D. A., Villarini, G., Cloke, H. L., Simmons, A., Roberts, N., Lombardi, A., Burgess, S. N., and Pappenberger, F.: How bad is the rain? Applying the extreme rain multiplier globally and for climate monitoring activities, Meteorological Applications, 32, e70 031, 2025.

Lenderink, G., Barbero, R., Loriaux, J. M., and Fowler, H. J.: Super-clausius-clapeyron scaling of extreme hourly convective precipitation and its relation to large-scale atmospheric conditions, Journal of Climate, 30, 6037–6052, https://doi.org/10.1175/JCLI-D-16-0808.1, 2017.

Li, L., Li, Y., and Li, Z.: Object-based tracking of precipitation systems in western Canada: the importance of temporal resolution of source data, Climate Dynamics, 55, 2421–2437, 2020.

Lionello, P. and Scarascia, L.: The relation between climate change in the Mediterranean region and global warming, Regional Environmental Change, 18, 1481–1493, https://doi.org/10.1007/s10113-018-1290-1, 2018.

Liu, P., Tsimpidi, A., Hu, Y., Stone, B., Russell, A., and Nenes, A.: Differences between downscaling with spectral and grid nudging using WRF, Atmospheric Chemistry and Physics, 12, 3601–3610, 2012.

Lombardo, K. and Bitting, M.: A Climatology of Convective Precipitation over Europe, Monthly Weather Review, 152, 1555 – 1585, https://doi.org/10.1175/MWR-D-23-0156.1, 2024.

Lussana, C., Baietti, E., Båserud, L., Nipen, T. N., and Seierstad, I. A.: Exploratory analysis of citizen observations of hourly precipitation over Scandinavia, Advances in Science and Research, 20, 35–48, 2023.

Lussana, C., Cavalleri, F., Brunetti, M., Manara, V., and Maugeri, M.: Evaluating long-term trends in annual precipitation: A temporal consistency analysis of ERA5 data in the Alps and Italy, Atmospheric Science Letters, p. e1239, https://doi.org/https://doi.org/10.1002/asl.1239, 2024.

Mann, H. B.: Nonparametric tests against trend, Econometrica: Journal of the econometric society, pp. 245–259, 1945.

Marzban, C. and Sandgathe, S.: Cluster analysis for verification of precipitation fields, Weather and Forecasting, 21, 824–838, 2006.

Mazzoglio, P., Butera, I., and Claps, P.: I2-RED: a massive update and quality control of the Italian annual extreme rainfall dataset, Water, 12, 3308, 2020.

Mazzoglio, P., Butera, I., Alvioli, M., and Claps, P.: The role of morphology in the spatial distribution of short-duration rainfall extremes in Italy, Hydrology and Earth System Sciences, 26, 1659–1672, 2022.

Mazzoglio, P., Viglione, A., Ganora, D., and Claps, P.: Mapping the uneven temporal changes in ordinary and extraordinary rainfall extremes in Italy, Journal of Hydrology: Regional Studies, 58, 102 287, https://doi.org/https://doi.org/10.1016/j.ejrh.2025.102287, 2025.

McLeod, A. I.: Kendall rank correlation and Mann-Kendall trend test, R package Kendall, 602, 1–10, 2005.

Morbidelli, R., Flammini, A., Echeta, O., Albano, R., Anzolin, G., Zumr, D., Badi, W., Berni, N., Bertola, M., Bodoque, J. M., Brandsma, T., Cauteruccio, A., Cesanelli, A., Cimorelli, L., Chaffe, P. L., Chagas, V. B., Dari, J., das Neves Ameida, C., Díez-Herrrero, A., Doesken, N., El Khalki, E. M., Saidi, M. E., Ferraris, S., Freitas, E. S., Gargouri-Ellouze, E., Gariano, S. L., Hanchane, M., Hurtado, S. I., Kessabi, R., Khemiri, K., Kim, D., Kowalewski, M. K., Krabbi, M., Lazzeri, M., Lompi, M., Mazzoglio, P., Meira, M. A., Moccia, B., Moutia, S., Napolitano, F., Newman, N., Pavlin, L., Peruccacci, S., Pianese, D., Pirone, D., Ricetti, L., Ridolfi, E., Russo, F., Sarochar, R. H., Segovia-Cardozo, D. A., Segovia-Cardozo, S., Serafeim, A. V., Sojka, M., Speranza, G., Urban, G., Versace, C., Wałęga, A., Zubelzu, S., and Saltalippi, C.: A reassessment of the history of the temporal resolution of rainfall data at the global scale, Journal of Hydrology, 654, 132 841, https://doi.org/https://doi.org/10.1016/j.jhydrol.2025.132841, 2025.

Padulano, R., Reder, A., and Rianna, G.: An ensemble approach for the analysis of extreme rainfall under climate change in Naples (Italy), Hydrological Processes, 33, 2020–2036, 2019.

Pavan, V., Antolini, G., Barbiero, R., Berni, N., Brunier, F., Cacciamani, C., Cagnati, A., Cazzuli, O., Cicogna, A., De Luigi, C., et al.: High resolution climate precipitation analysis for north-central Italy, 1961–2015, Climate Dynamics, 52, 3435–3453, 2019.

Peleg, N., Koukoula, M., and Marra, F.: A 2°C warming can double the frequency of extreme summer downpours in the Alps, npj Climate and Atmospheric Science, 8, 216, https://doi.org/10.1038/s41612-025-01081-1, 2025.

Persiano, S., Ferri, E., Antolini, G., Domeneghetti, A., Pavan, V., and Castellarin, A.: Changes in seasonality and magnitude of sub-daily rainfall extremes in Emilia-Romagna (Italy) and potential influence on regional rainfall frequency estimation, Journal of Hydrology: Regional Studies, 32, 100 751, 2020.

Pfahl, S., O'Gorman, P. A., and Fischer, E. M.: Understanding the regional pattern of projected future changes in extreme precipitation, Nature Climate Change, 7, 423–427, https://doi.org/https://doi.org/10.1038/nclimate3287, 2017.

Poschlod, B., Ludwig, R., and Sillmann, J.: Ten-year return levels of sub-daily extreme precipitation over Europe, Earth System Science Data, 13, 983–1003, https://doi.org/10.5194/essd-13-983-2021, 2021.

Raffa, M., Reder, A., Marras, G. F., Mancini, M., Scipione, G., Santini, M., and Mercogliano, P.: VHR-REA_IT Dataset: Very High Resolution Dynamical Downscaling of ERA5 Reanalysis over Italy by COSMO-CLM, Data, 6, https://doi.org/10.3390/data6080088, 2021.

Schroeer, K., Kirchengast, G., and O, S.: Strong Dependence of Extreme Convective Precipitation Intensities on Gauge Network Density, Geophysical Research Letters, 45, 8253–8263, https://doi.org/https://doi.org/10.1029/2018GL077994, 2018.

Sen, P. K.: Estimates of the Regression Coefficient Based on Kendall's Tau, Journal of the American Statistical Association, 63, 1379–1389, https://doi.org/10.1080/01621459.1968.10480934, 1968.

Senatore, A., Furnari, L., Nikravesh, G., Castagna, J., and Mendicino, G.: Increasing Daily Extreme and Declining Annual Precipitation in Southern Europe: A Modeling Study on the Effects of Mediterranean Warming, EGUsphere, https://doi.org/10.5194/egusphere-2025-1567, preprint, 2025.

Sottile, G., Francipane, A., Adelfio, G., and Noto, L. V.: A PCA-based clustering algorithm for the identification of stratiform and convective precipitation at the event scale: an application to the sub-hourly precipitation of Sicily, Italy, Stochastic Environmental Research and Risk Assessment, 36, 2303–2317, 2022.

Stocchi, P. and Davolio, S.: Intense air-sea exchanges and heavy orographic precipitation over Italy: The role of Adriatic sea surface temperature uncertainty, Atmospheric Research, 196, 62–82, 2017.

Thunis, P. and Bornstein, R.: Hierarchy of Mesoscale Flow Assumptions and Equations, Journal of Atmospheric Sciences, 53, 380 – 397, https://doi.org/10.1175/1520-0469(1996)053<0380:HOMFAA>2.0.CO;2, 1996.

Van Hyfte, S., Le Moigne, P., Bazile, E., Verrelle, A., and Boone, A.: High-Resolution Reanalysis of Daily Precipitation using AROME Model Over France, Tellus A: Dynamic Meteorology and Oceanography, https://doi.org/10.16993/tellusa.95, 2023.

Viterbo, F., Sperati, S., Vitali, B., D'Amico, F., Cavalleri, F., Bonanno, R., and Lacavalla, M.: MERIDA HRES: A new high-resolution reanalysis dataset for Italy, Meteorological Applications, 31, e70 011, 2024.

von Storch, H., Langenberg, H., and Feser, F.: A Spectral Nudging Technique for Dynamical Downscaling Purposes, Monthly Weather Review, 128, 3664 – 3673, https://doi.org/10.1175/1520-0493(2000)128<3664:ASNTFD>2.0.CO;2, 2000.

Wang, S., Li, C., Li, D., Tian, X., Bao, H., Chen, G., and Xia, Y.: Exploring the utility of radar and satellite-sensed precipitation and their dynamic bias correction for integrated prediction of flood and landslide hazards, Journal of Hydrology, https://doi.org/https://doi.org/10.1016/j.jhydrol.2021.126964, 2021.

Wernli, H., Paulat, M., Hagen, M., and Frei, C.: SAL—A novel quality measure for the verification of quantitative precipitation forecasts, Monthly Weather Review, 136, 4470–4487, 2008.

White, R., Battisti, D., and Skok, G.: Tracking precipitation events in time and space in gridded observational data, Geophysical Research Letters, 44, 8637–8646, 2017.

Wilks, D.: On "field significance" and the false discovery rate, Journal of applied meteorology and climatology, 45, 1181–1189, 2006.

Wilks, D.: Statistical Methods in the Atmospheric Sciences, Elsevier Science, ISBN 9780128158234, 2019.

Wilks, D. S.: "The Stippling Shows Statistically Significant Grid Points": How Research Results are Routinely Overstated and Overinterpreted, and What to Do about It, Bulletin of the American Meteorological Society, 97, 2263 – 2273, https://doi.org/10.1175/BAMS-D-15-00267.1, 2016.

Zaitchik, B. F., Rodell, M., Biasutti, M., and Seneviratne, S. I.: Wetting and Drying Trends Under Climate Change, Nature Water, 1, 502–513, https://doi.org/10.1038/s44221-023-00073-w, 2023.